Phosphorylation of the overlooked tyrosine 310 regulates the structure, aggregation, and microtubule- and lipid-binding properties of Tau

Nadine Ait-Bouziad [1], Anass Chiki [1], Galina Limorenko [1], Shifeng Xiao [2], David Eliezer [3], and Hilal A. Lashuel [1*]

From the [1]Laboratory of Molecular and Chemical Biology of Neurodegeneration, Brain Mind Institute, École Polytechnique Fédérale de Lausanne (EPFL), CH-1015 Lausanne, Switzerland; [2]Shenzhen Key Laboratory of Marine Biotechnology and Ecology, College of Life Sciences and Oceanography, Shenzhen University, Shenzhen, 518060, China; [3]Department of Biochemistry and Program in Structural Biology, Weill Cornell Medical College , New York, New York 10065, United States

Running title: *Phosphorylation at Y310 regulates Tau biophysical properties*

*To whom correspondence should be addressed: Hilal A. Lashuel: Laboratory of Molecular and Chemical Biology of Neurodegeneration, Brain Mind Institute, École Polytechnique Fédérale de Lausanne (EPFL), CH-1015 Lausanne, Switzerland; Hilal.lashuel@epfl.ch; Tel. +41216939691, Fax. +41216939665,

Keywords : Tau protein (Tau), tyrosine phosphorylation, phosphotyrosine, Y310, aggregation, microtubule, lipid.

ABSTRACT

The microtubule-associated protein Tau is implicated in the pathogenesis of several neurodegenerative disorders, including Alzheimer's disease. Increasing evidence suggest that post-translational modifications play critical roles in regulating Tau normal functions and its pathogenic properties in tauopathies. Very little is known about how phosphorylation of tyrosine residues influences the structure, aggregation, microtubule- and lipid-binding properties of Tau. In this work, we aimed to address this knowledge gap and determine the relative contribution of phosphorylation of one or several of the five tyrosine residues in Tau (Y18, Y29, Y197, Y310 and Y394) to the regulation of its biophysical and functional properties. Towards this goal, we used a combination of site-specific mutagenesis and in vitro phosphorylation by c-Abl kinase to generate Tau species phosphorylated at all tyrosine residues, except Y310 or Y394 (pTau-Y310F, pTau-Y394F) and tau phosphorylated only at Y310 and Y394 (4F\pY310 or 4F\pY394). Our results show that phosphorylation at all five tyrosine residues, multiple N-terminal tyrosine residues (Y18, Y29 and Y197) or site-specific phosphorylation at residue Y310, itself located in the microtubule-binding and aggregation-prone domain of Tau was sufficient to abolish Tau aggregation and inhibit its microtubule- and lipid-binding properties. NMR studies demonstrated that these effects were mediated by a local decrease in β−sheet propensity of PHF6 domain. Our findings underscore the unique role of Y310 phosphorylation and highlight the importance of further studies to elucidate its role in tauopathies and its role in regulating Tau function in health and disease.

INTRODUCTION

The misfolding and aggregation of the microtubule (MT)-associated protein Tau have been linked to the pathogenesis of several neurodegenerative disorders, including Alzheimer disease (AD), corticobasal degeneration (CBD), progressive supranuclear palsy (PSP), Pick's disease (PiD), argyrophilic grain disease (AGD), chronic traumatic encephalopathy (CET) and frontotemporal dementia with parkinsonism linked to chromosome 17 (FTDP-17) (1-7). In the brain of individuals affected by AD, aggregated and abnormally hyper-phosphorylated and modified forms of Tau, such as paired helical filaments (PHFs) and straight filaments (SFs), are found as the main component of the neurofibrillary tangles (NFTs), one of the key diagnostic pathological hallmarks of AD, in addition to amyloid plaques (8).

Tau is extensively post-translationally modified (PTM) with phosphorylation being one of the predominant modification (9). Although many phosphorylation sites of Tau identified in NFTs are also found in healthy neurons, at advanced disease stages Tau aberrant hyper-phosphorylation (10) encompasses more than 39 potential sites (11,12), leading to a total phosphorylation level of Tau that is three to four times higher than that of normal Tau (13,14). The presence of hyper-phosphorylated Tau in both soluble cytosolic form and highly aggregated and insoluble forms within NFTs (13,15) suggests that the pattern of hyper-phosphorylation or sites-specific phosphorylation may play key roles in regulating its normal function(s) and/or pathogenic properties.

Serine and threonine residues greatly outnumber tyrosine residues in the Tau sequence, which explains why phosphorylation at these residues has received predominant attention. However, Tau contains five tyrosine residues (Figure 1), located at positions Y18, Y29, Y197, Y310 and Y394, which are all susceptible to phosphorylation. Tau phosphorylation on tyrosine residues has been described only recently and remains understudied. A few tyrosine kinases have been shown to phosphorylate tyrosine residues in Tau both *in vitro*, in cell culture and *in vivo*. For example, Fyn (16,17) and Lck (17) members of the Src kinase family phosphorylated Tau on all five tyrosine residues, however somewhat preferentially on residue Y18; while members of the c-Abl kinase family (c-Abl and Arg) were reported to phosphorylate Tau on Y394 (18,19) and to a lesser extent on Y197 and Y310. Other non-SH3-containing tyrosine kinases have also been reported to phosphorylate Tau on residue Y18, such as Syk (20) and recently described Pyk2, the focal adhesion kinase (FAK) family member that is also regulated by Fyn (21); and on residue Y197 by TTBK1 (22). Additionally, it was shown that an increase in Tau tyrosine phosphorylation correlated with the

formation of Tau aggregates (23). Furthermore, several reports have established that Abelson tyrosine kinase (c-Abl) becomes active in a variety of neurodegenerative diseases, including Parkinson's disease (PD) and several Tauopathies (24-26), suggesting a likely role in the regulation of Tau tyrosine phosphorylation levels in disease. Whereas phosphorylation of serine and threonine residues exhibit a degree of clustering in the N- and C-terminal functional domains encompassing the repeat regions, as well as MT-binding domains 1 and 2 (Figure 1, A), there is only one tyrosine phosphorylation site (Y310) within the MT-binding domain, in the repeat peptide R3, which has also been shown to play key roles in regulating Tau aggregation, PHF formation, and membrane interactions (27,28).

Interestingly, despite the prominent position of Y310 within the aggregation-prone hexapeptide PHF6 (amino acids 306-311), only a handful of studies have specifically investigated the roles of tyrosine 310 in regulating Tau structure, aggregation, and toxicity. Importantly, none of the previous studies (29-37) specifically investigated the effects of Y310 phosphorylation in the context of the full-length Tau protein, relying instead on the short PHF6-containing peptides, featuring PHF6-derived sequences as short as 3 amino acids (38). Santa-Maria *et al.* (39) showed that phosphorylation of Y310 abolished the aggregation of the PHF6 fragment (amino acids 306-311) *in vitro*. Conversely, Inoue *et al*. reported contradictory results, where substitution of Y310 with non-natural derivatives 4-phenylphenylalanine and 4-methylphenylalanine, as well as phosphorylation of Y310 resulted in a marked increase in the propensity of PHF6 peptide to form fibrils (34,40,41). In addition, most studies used tyrosine 310 amino acid substitutions to alanine, non-physiological buffer conditions, as well as cofactors such as trimethylamine N-oxide to gain insights on Y310 contribution to PHF6-containing domain aggregation. All these conditions may not correctly recapitulate the PHF6-dependent aggregation properties of full-length Tau (42). Furthermore, while previous studies have suggested that Tau phosphorylation on tyrosine residues is an important modulator of Tau functions under both normal conditions and in the course of AD pathogenesis (16,43), the role of each individual tyrosine residue in regulating Tau protein aggregation, MT-binding, and lipid-binding propensities has not been systematically investigated.

This knowledge gap combined with the location of Y310 within the PHF6 domain Tau prompted us to conduct more detailed investigations to 1) determine the effects of tyrosine phosphorylation on regulation of the normal function and pathogenic properties of full-length Tau; 2) elucidate the relative contribution of phosphorylation at each tyrosine residue; and 3) investigate the effect of phosphorylation at Y310 on the structure, aggregation and microtubule-binding of the full-length Tau and microtubule-binding domain-

containing Tau K18 fragment. Towards achieving these goals, we utilized a combination of mutagenesis and *in vitro* phosphorylation using the c-Abl kinase to produce milligram quantities of Tau phosphorylated at single or multiple tyrosine residues. Our findings show that phosphorylation of Y310 is sufficient to inhibit Tau aggregation and plays a key role in regulating Tau microtubule-binding properties and interactions with the membrane, thus underscoring the importance of further studies to elucidate the role of phosphorylation at this residue in regulating Tau function under normal and pathological conditions.

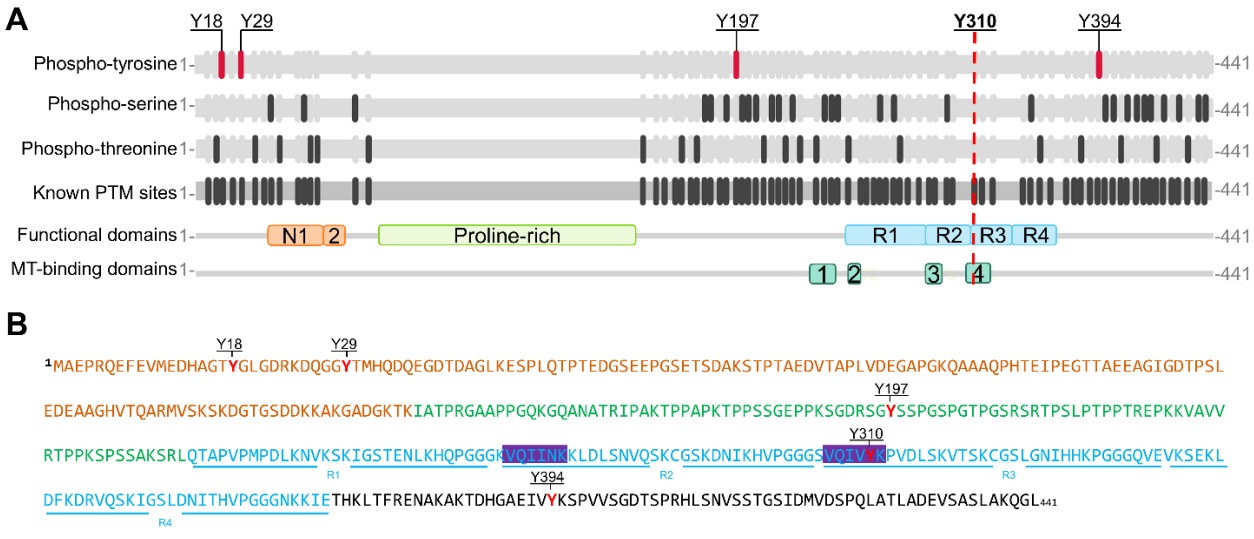

Figure 1. Full-length Tau-441 map and sequence. (A) Map and domains of full-length Tau with known post-translational modification sites (grey); phospho-tyrosines (pY, magenta), phospho-serines (pS, dark grey) and phospho-threonines (pT, dark grey). Furthermore, Tau contains different functional domains: N-terminal sites (N1,2), a proline-rich region, and four repeat domains (R1 aa 244-274; R2 aa 275-305; R3 aa 306-336; R4 aa 337-368). Microtubule-binding region (MTBR) contains 2 hexapeptide domains PHF6* (275-280) and PHF6 (306-311). Adapted from http://www.Tauptm.org (74). **(B)** The annotated sequence of full-length Tau. Tau possesses 5 tyrosine residues, as indicated in red, at positions Y18, Y29, Y197, Y310 and Y394. Y18 and Y29 are localized in the N-terminal Tau inserts (orange), Y197 in the proline-rich domain, Y310 in the third repeat of the MTBR of Tau (blue) and Y394 in the C-terminal part of the protein (black). PHF6 and PHF6* hexapeptides are indicated in purple.

RESULTS

c-Abl phosphorylates Tau on multiple tyrosine residues *in vitro*.

To investigate the role of tyrosine phosphorylation in regulating Tau structure, aggregation and MT-binding properties, we first sought to develop conditions that allow for efficient phosphorylation of Tau *in vitro*. Towards this goal, we assessed the phosphorylation efficiency and specificity of c-Abl kinase for Tau. Recombinant full-length Tau was subjected to *in vitro* phosphorylation using recombinant c−Abl and the extent of phosphorylation and number of phosphorylation events was systematically followed by ESI/MS. Fig. 2, A shows that c-Abl phosphorylated Tau at multiple sites, up to 5 sites after 4 h of incubation in reaction buffer. Increasing the amount of kinase or incubation time did not lead to a further increase in the number of phosphorylation sites or phosphorylation levels (data not shown).

Although RP−HPLC allowed the separation of the kinase from the phosphorylated Tau proteins, it was not possible to achieve separation of the different phosphorylated species and all the different phosphorylated forms of Tau eluted in one peak during as observed by the UPLC of the C-abl phosphorylated Tau (Figure 3, B) where all the species eluted as one single peak. To determine the exact tyrosine phosphorylation profile of Tau, the purified mixture of pTau was digested by trypsin and the resulting peptides were analyzed by LC/MS/MS. The analysis of the phosphorylated sites was performed using the Scaffold software (http://www.proteomesoftware.com/) which determines the abundance of phosphorylated peptides based on the spectral counting (SP). As shown in Fig. 2, D-E, c−Abl phosphorylated Tau on Y18, Y29, Y197, Y310 and Y394, with Y310 and Y394 being the major phosphorylation sites.

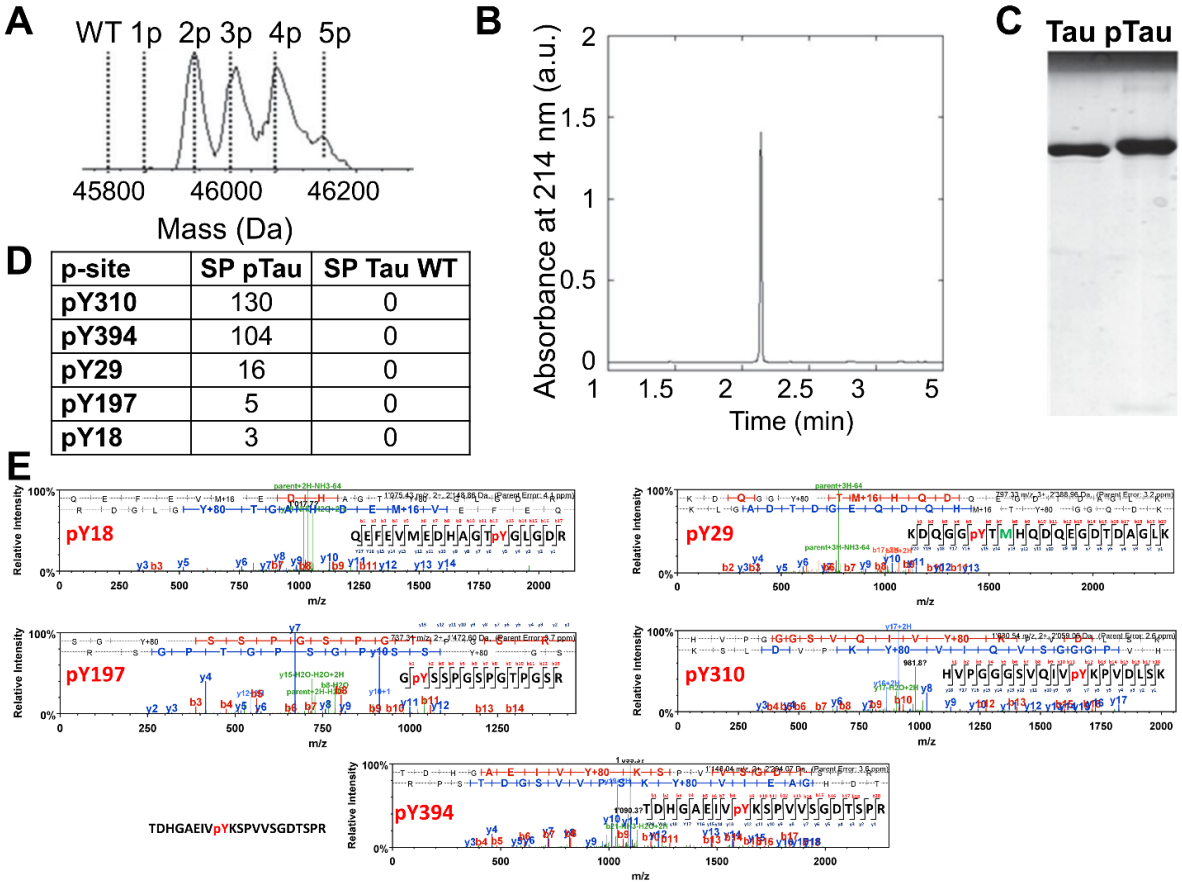

p-site	SP pTau	SP Tau WT
pY310	130	0
pY394	104	0
pY29	16	0
pY197	5	0
pY18	3	0

Figure 2. Detailed characterization of Tau phosphorylated by c-Abl. Phosphorylated Tau by C-abl (pTau; phosphorylation was performed for 4 h, which leads to a mixture of Tau phosphorylated on two to five residues) was characterized after RP-HPLC by LC-MS **(A)**, UPLC **(B)** and SDS-PAGE **(C)**, LC−MS spectra of phosphorylated Tau, UPLC chromatogram and SDS-PAGE of purified Tau following phosphorylation by c−Abl. **(D-E)** Purified pTau was digested by trypsin and the resulting peptides enriched using a TiO_2 resin and subsequently analyzed by tandem LC/MS/MS. The analysis of the phosphopeptides was performed using the Scaffold version 4.0 (Proteome Software), and the number of phosphopeptides detected per phosphorylation site was reported as the spectral count (SP).

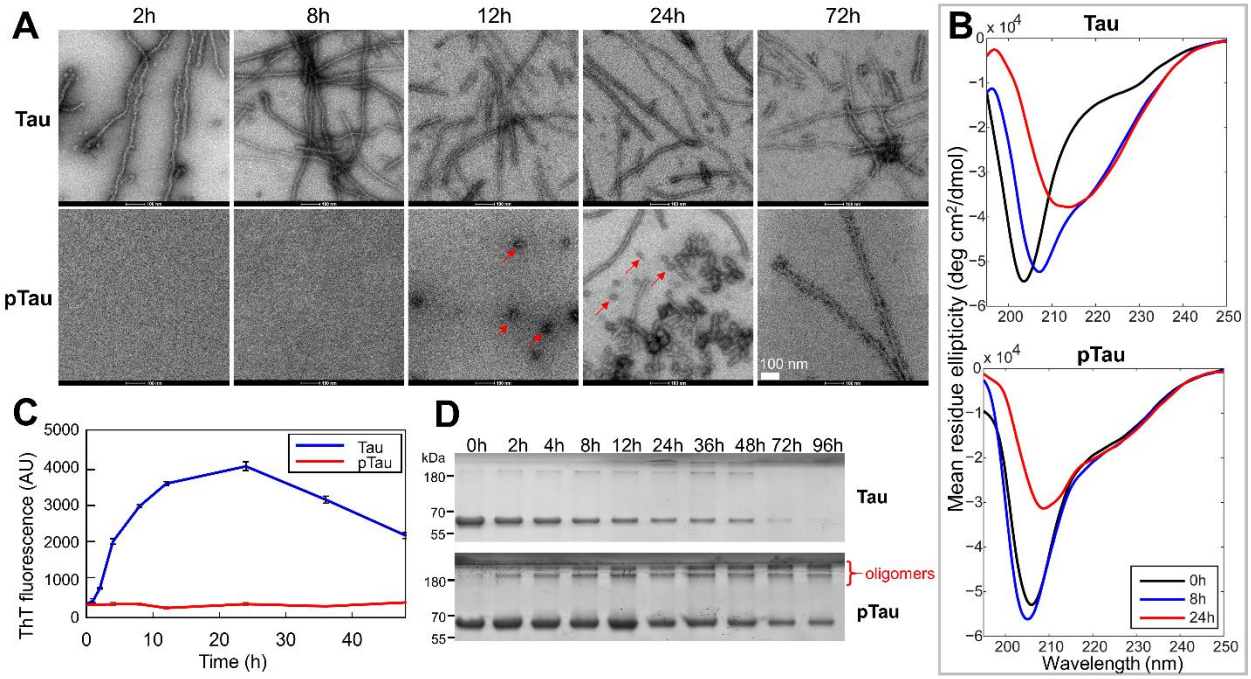

Figure 3 Aggregation behavior of non-phosphorylated Tau compared to phosphorylated pTau. 10 µM Tau and pTau were incubated for several days at 37°C under shaking conditions, in presence of 2.5 µM heparin. **(A)** EM micrographs of Tau (top panels) and pTau (bottom panels) at different aggregation times. While Tau protein readily formed fibrillar structures, Tau phosphorylated by c-Abl formed many large oligomeric structures (red arrows), as well as a few fibrils. Scale bar overlaid for clarity. **(B)** CD spectra recorded at different time points showed that Tau protein fully converted into β−sheet-containing structures after 24 h, while the pTau contained mostly random coil. **(C)** ThT fluorescence was measured at different time points, Tau phosphorylated by c−Abl did not induce any increase in ThT fluorescence after 48 h of incubation. **(D)** At several time points, an aliquot of the aggregation reaction was taken and centrifuged. The supernatants were run on SDS−PAGE gel. Tau protein showed a decrease in the soluble fraction over time, while the decrease observed in the soluble fraction of monomeric pTau was accompanied by an increasing amount of oligomeric pTau species (highlighted in red). Quantification of the supernatant band intensity could not be performed due to the presence of soluble non−pelletable oligomeric species in the pTau sample.

c-Abl-phosphorylation of Tau significantly delays its aggregation.

To determine the effect of tyrosine phosphorylation on Tau aggregation, we carried out *in vitro* phosphorylation of Tau using the c-Abl kinase and purified the mixture of Tau phosphorylated proteins using RP-HPLC. Next, we compared *in vitro* aggregation of the non-phosphorylated to c-Abl-phosphorylated Tau (Fig. 3) by incubating 10 µM of protein for two days at 37°C under shaking conditions, in presence of 2.5 µM heparin. We found that phosphorylated Tau (pTau) was unable to form canonical β−sheet-containing fibrils, as demonstrated by the fact that the ThT fluorescence remained at baseline levels (Fig. 3, C) and the absence of conversion of Tau conformation to β−sheet structure as discerned by circular dichroism (CD) (Fig. 3, B). However, large oligomers were discernible by electron microscopy at 12 h, and longer fibrils were apparent after 24-48 h incubation, as confirmed by the fact that the sedimentation assay showed an increase of the oligomeric species overtime in the pTau sample (Fig. 3, A, D). These results demonstrate that phosphorylation of Tau at multiple tyrosine residues significantly delays its aggregation and fibril formation and results in the accumulation of Tau oligomers.

c-Abl-mediated inhibitory effects on Tau aggregation depend on the site of tyrosine phosphorylation.

To determine the relative contribution of each tyrosine residue to the c-Abl phosphorylation-mediated inhibition of Tau aggregation, we sought to generate Tau proteins that are phosphorylated or not at one or a selected number of tyrosine residues focusing on Y394 and Y310. To allow site-specific phosphorylation of these residues, we mutated all tyrosine residues except Y310 (4F\Y310) or Y394 (4F\Y394) to phenylalanine. In addition, we generated Y310 and Y394 residue-specific phosphorylation deficient Tau mutants, where each of these residues is mutated to phenylalanine to allow phosphorylation of all other tyrosine residues except at Y310 (Y310F) or Y394 (Y394F) (Fig. 4, A, hollow circles). All of these Tau variants were subjected to *in vitro* phosphorylation using c-Abl (Fig. 4, A, red circles) and the phosphorylated proteins were purified and their aggregation properties were compared to that of the corresponding non-phosphorylated variants. For the 4F\Y310 and 4F\Y394 mutants, which can only be phosphorylated at Y310 and Y394, complete phosphorylation was achieved, whereas a mixture of up to four phosphorylation sites was observed for the single Y310F and Y394F mutants (see LC−MS spectra in Table 1). We next investigated the kinetics of aggregation of Tau Y−>F mutants using the same experimental conditions as for full-length Tau (Fig. 4). We observed that 4F\pY310, pTau−Y310F and pTau−Y394F were unable to aggregate, as demonstrated by the lack of increase in the ThT fluorescence for these samples (Fig. 4, D), while 4F\pY394 retained its capacity to form β−sheet-containing species. These findings were supported by EM data (Fig. 4, B), where only the 4F\pY394 sample was found to

contain Tau of fibrillar morphology, whereas all other phosphorylated mutants only showed the presence of oligomeric species (Fig. 4, D, arrows). These results were further supported by the sedimentation assay, whereupon removal of fibrillar species by ultracentrifugation monomeric Tau species showed time-dependent decrease in soluble Tau in all non-phosphorylated mutants (Fig. 4, C) that parallels the increase in ThT fluorescence signal (Fig. 4, D), signifying the recruitment of monomeric Tau into β−sheet-containing species. Time-dependent decrease in monomeric Tau over time was also observed for phosphorylated Tau mutants, however in contrast to their non-phosphorylated counterparts or mutant 4F\pY394, higher molecular weight Tau bands were apparent for phosphorylated Tau mutants 4F\pY310, pTau−Y310F and pTau−Y394F (Fig. 4, C, red boxes), suggesting the presence of Tau oligomeric species, which is in agreement with EM and ThT data. These findings suggest that phosphorylation at Y310, but not Y394 is sufficient to inhibit the fibrillization of Tau, as 4F\pY394 was able to aggregate to the same extent as its non−phosphorylated version. Interestingly, phosphorylation of the Y310F mutant also suppressed Tau fibril formation, even though in this mutant the residue Y310 is absent and not available for phosphorylation, indicating that phosphorylation of N-terminal tyrosine residues Y18, Y29 and Y197 may also play important role in inhibiting Tau aggregation, possibly through mechanisms different to the expected direct pY310-induced conformational shift of PHF6 domain (see below). These results show that although Y310 phosphorylation is sufficient to suppress the aggregation of the full-length Tau, the synergistic interplay between phosphorylation of the other tyrosine residues is also of critical importance in modulating Tau oligomerization and fibril formation.

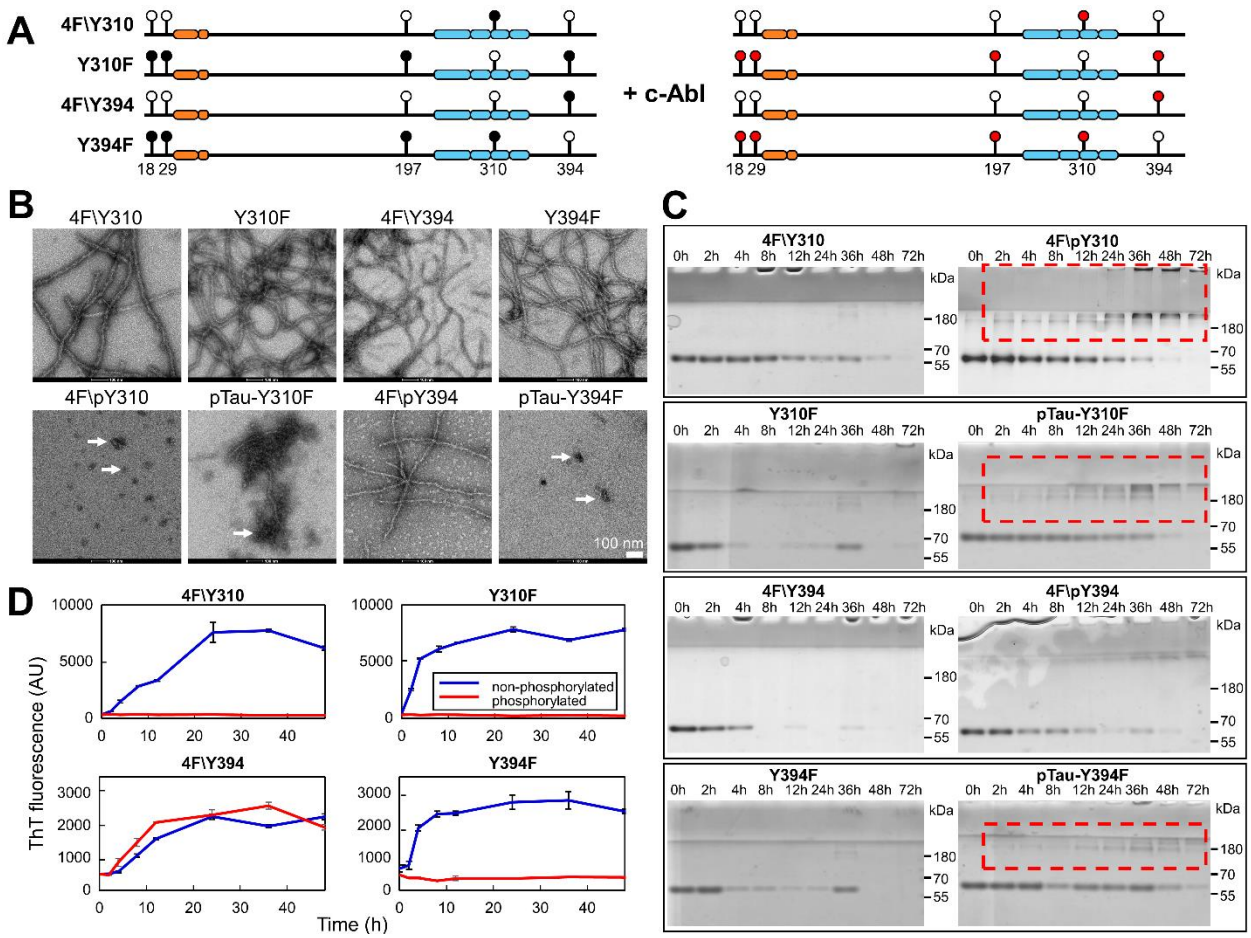

Figure 4. Aggregation behavior of non-phosphorylated compared to phosphorylated Y->F Tau mutants. 10 µM non- and phosphorylated Y−>F Tau mutants were incubated for several days at 37°C under shaking conditions, in the presence of 2.5 µM heparin. **(A)** Schematic showing the position of Tau tyrosine residue mutations (filled circle: Y; hollow circle: F) and stoichiometry of the phosphorylated sites by c-Abl (red circles). **(B)** EM micrographs of non-phosphorylated (top panels) and phosphorylated (bottom panels) Tau Y−>F mutants at 24 h. The non−phosphorylated Tau mutants formed fibrils efficiently. Of the phosphorylated proteins only the 4F\pY394 was able to form fibrils efficiently, while 4F\p3Y10, pTau−Y310F and pTau−Y394F formed many oligomeric and amorphous structures (red arrows). **(C)** ThT fluorescence was measured at different time points and reported as a ThT kinetics (graphs showing one representative example for each mutant). The non−phosphorylated mutants all showed a comparable increase in ThT fluorescence over time. Of the phosphorylated proteins only the 4F\pY394 was able to form cross−β−rich structures, as detected by the increase in ThT fluorescence over time. Conversely, 4F\p3Y10, pTau−Y310F and pTau−Y394F did not induce any increase in ThT over 48 h of incubation. **(D)** At several time points, an aliquot of the aggregation was taken and centrifuged. The supernatants were run on SDS−PAGE. The non−phosphorylated mutants all showed a significant reduction of the soluble fraction over time. Out of the phosphorylated proteins only the 4F\pY394 presented a similar reduction in the amount of soluble protein over time, while the 4F\p3Y10, pTau−Y310F and pTau−Y394F formed non−pelletable oligomeric structures (red dashed rectangles).

Table 1. Denomination and characteristics of the recombinant proteins used in this study. From left to right; the name of phosphorylated protein, definition, level of phosphorylation achieved by c−Abl and corresponding LC−MS spectra.

Name of phosphorylated protein	Definition	Level of phosphorylation	LC-MS of c-Abl phosphorylated protein
pK18	WT 4R domain of Tau and phosphorylated in vitro with c-Abl	100% mono-phosphorylated on Y310	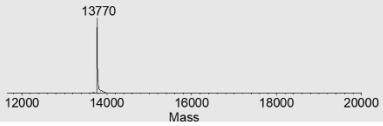
pK18 13C 15N	WT 4R domain of Tau isotopically labelled with 13C and 15N phosphorylated *in vitro* with c-Abl	100% mono-phosphorylated on Y310	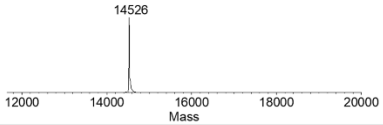
pTau	WT 4R2N Tau	Phosphorylated (mixture) on all tyrosines	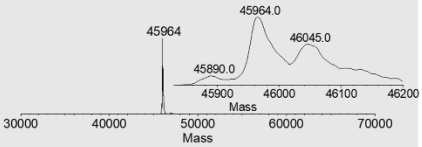
pTau-Y310F	Y->F at position 310 WT phosphorylated in vitro with c-Abl	Phosphorylated (mixture) on all tyrosines except Y310	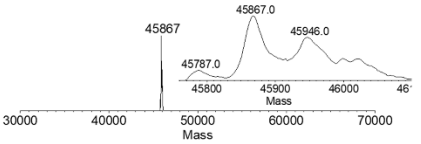
4F/pY310	Y->F at positions 18,29, 197 and 394 phosphorylated in vitro with c-Abl	100% mono-phosphorylated on Y310	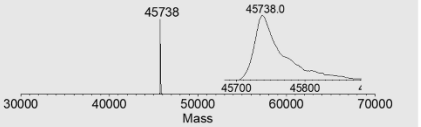
pTau-Y394F	Y->F at position 394 phosphorylated in vitro with c-Abl	Phosphorylated (mixture) on all tyrosines except Y394	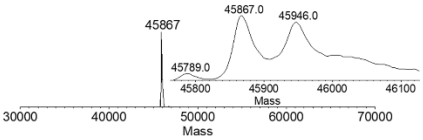
4F/pY394	Y->F at positions 18, 29, 197 and 310 phosphorylated in vitro with c-Abl	100% mono-phosphorylated on Y394	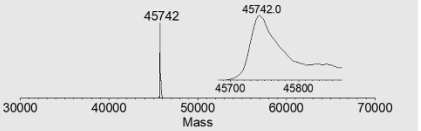

Tyrosine 310 phosphorylation underlies the structural basis of the inhibitory effect on Tau aggregation.

The strong inhibitory effects of Y310 phosphorylation combined with the fact that it represents the only tyrosine residue within the MT-binding domain of full-length Tau and K18 fragment prompted us to investigate the molecular and structural bases by which Y310 phosphorylation inhibits Tau aggregation propensity. Towards this goal, we performed nuclear magnetic resonance (NMR) studies on the K18 peptide, which encompasses the MT-binding region (residues 244-368 of Tau-441 sequence) and includes the highly amyloidogenic PHF6 and PHF6* hexapeptides, the latter of which contains Y310 (Fig. 1). K18 is also known for its high propensity to aggregate *in vitro* (44).

To this end, we produced recombinant 15N-labelled K18 and subjected it to *in vitro* phosphorylation using recombinant c−Abl under the same experimental conditions as for full-length Tau. Given that there is only one tyrosine residue in K18, we were able to achieve complete K18 phosphorylation on Y310 within 4 h and obtained highly pure Y310-specifically modified pK18 (Fig. 5, A-C).

Next, to determine the effect of tyrosine 310 phosphorylation on the structural properties of K18, we performed NMR analysis of 15N-labeled pK18. The proton−nitrogen HSQC spectrum of pK18 compared to that of K18 showed that phosphorylation at residue Y310 induced local effects on the structure of the peptide, as indicated by chemical shift changes for signals originating from residues surrounding Y310 (Fig. 5, D). Interestingly, signals that were affected in the spectrum of pK18 consistently moved towards lower 15N chemical shifts. Because increases/decreases in NMR 15N chemical shifts correlate with increases/decreases in local β-strand structure (45), the observed decrease in 15N chemical shifts upon Y310 phosphorylation indicate a local decrease in β-sheet propensity for the PHF6 region as well as the subsequent ~10 residues (Fig. 5, E). This effect likely results from the added negative charges of the phosphate group. Notably, the affected region adopts β-sheet conformations in all known Tau fibril structures. Thus local decrease in β-sheet propensity may have important implications in the context of Tau fibrillization, especially as the PHF6 hexapeptide exhibits the strongest intrinsic β-sheet propensity in the Tau sequence (46) and is critical for the aggregation of the protein (36,47).

To further test whether Y310 phosphorylation impacted K18 aggregation, we performed *in vitro* aggregation of Y310 phosphorylated K18 (Fig. 6) by incubating 10 µM of protein for several days at 37°C under shaking conditions, in the presence of 2.5 µM heparin.

We observed, as suggested by NMR data, that the aggregation of pK18 was significantly delayed compared to unmodified K18. In fact, both the ThT (Fig. 6, A) and the sedimentation assays (Fig. 6, D) showed a delay of about 2 h in the fluorescence increase and loss of soluble protein, respectively. Interestingly, the final absolute value of the plateau ThT signal of the phosphorylated K18 was consistently about two to three times higher than that of K18 peptide, suggesting a difference in fibril structure, packing of the fibrils or susceptibility to fragmentation, which may affect ThT binding capacity and thus the end-point ThT value.

To further investigate the effect of phosphorylation at Y310 on the early formation of β-sheet-containing species of K18, we monitored changes in K18 secondary structure overtime under aggregation conditions by CD spectroscopy. While K18 fully converted to β−sheet within 1 h, pK18 clearly showed markedly delayed conformational shift toward β−sheet spectra during 4 h of incubation (Fig. 6, B). EM confirmed that fibril formation by pK18 was also delayed and shows presence of oligomeric amorphous aggregates at early and intermediate time points (Fig. 6, C, 0.5 h, 1 h, 6 h:arrows), as well as predominantly a protofibril−like morphology during intermediate time points (Fig. 6, C, 1 h, 6 h), and a fully fibrillar morphology only at later time points (Fig. 6, C, 24 h). These findings suggest that Y310 phosphorylation plays an inhibitory role during the nucleation phase of K18 aggregation, as demonstrated by attenuation of the pK18 conformational change (Fig. 6, B) and delayed formation of β−sheet-containing structures (Fig. 6, A, C). Our data suggest that Y310 phosphorylation of K18 facilitates a K18 aggregation pathway that may be divergent from canonical β−sheet-driven fibrillization, thus favouring the formation of oligomeric species during the early time points.

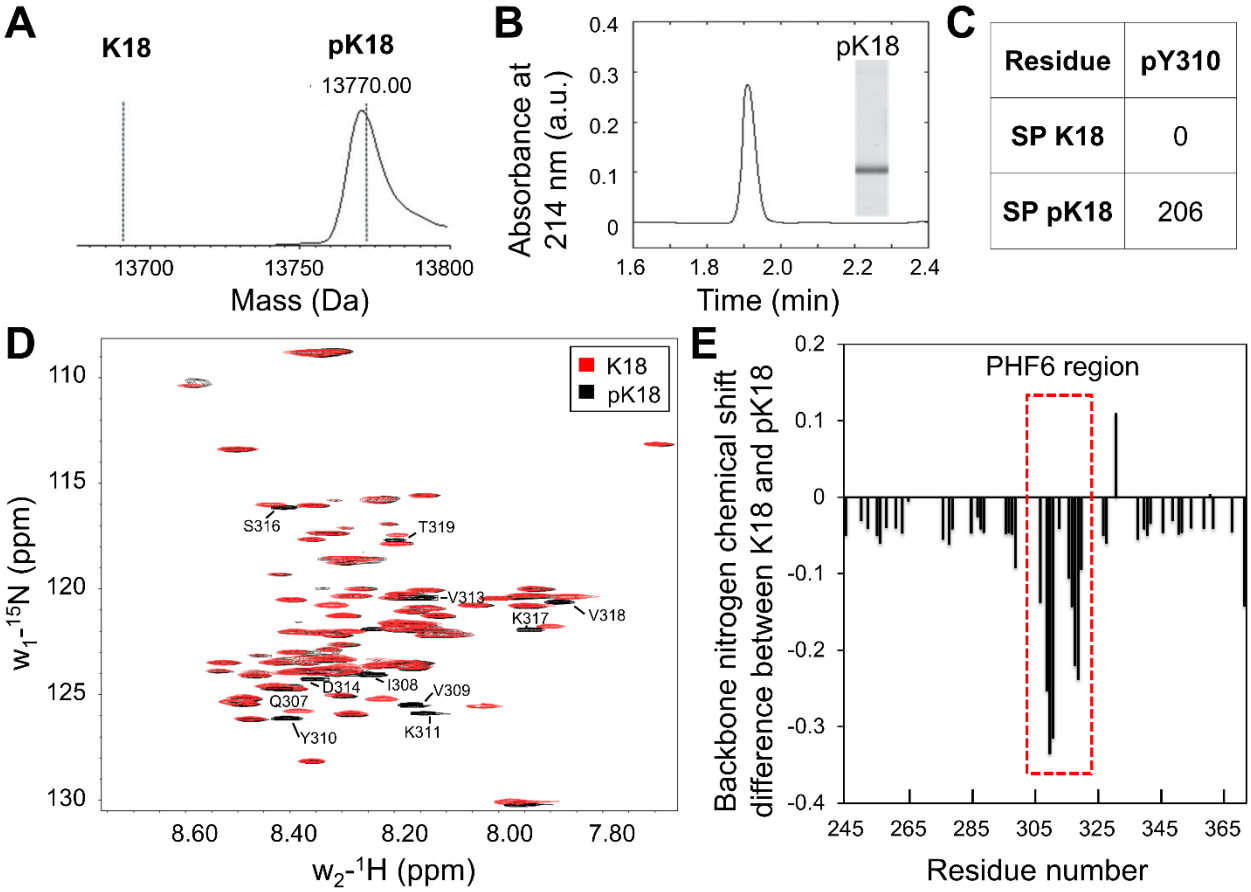

Figure 5. Detailed characterization of pK18 phosphorylated by c-Abl and NMR analysis of 15N pK18 compared to the non-phosphorylated K18. (A) LC−MS spectra, **(B)** UPLC profile and SDS-PAGE of reverse-phase HPLC of purified pK18 following phosphorylation by c−Abl (phosphorylation was performed for 4 h). K18 phosphorylated by c−Abl leads to the complete phosphorylation at residue Y310. Both K18 and pK18 were purified by reverse−phase HPLC to remove excess kinases. **(C)** The analysis of the phosphopeptides was performed using the Scaffold version 4.0 (Proteome Software), and the number of phosphopeptides detected per phosphorylation site was reported as the spectral count (SP). **(D)** Proton−nitrogen HSQC spectrum of unmodified K18 (black) compared to that of pK18 (red). Phosphorylation on Y310 induced local effects on the structure of pK18, as shown by chemical shift changes to annotated signals. **(E)** Decreased values of nitrogen chemical shifts (plotted as pK18 minus K18) indicate that phosphorylation decreases the β−sheet propensity of K18 in the PHF6 region, as well as for the subsequent ~10 residues, all of which are found in a β-sheet conformations in Tau fibrils.

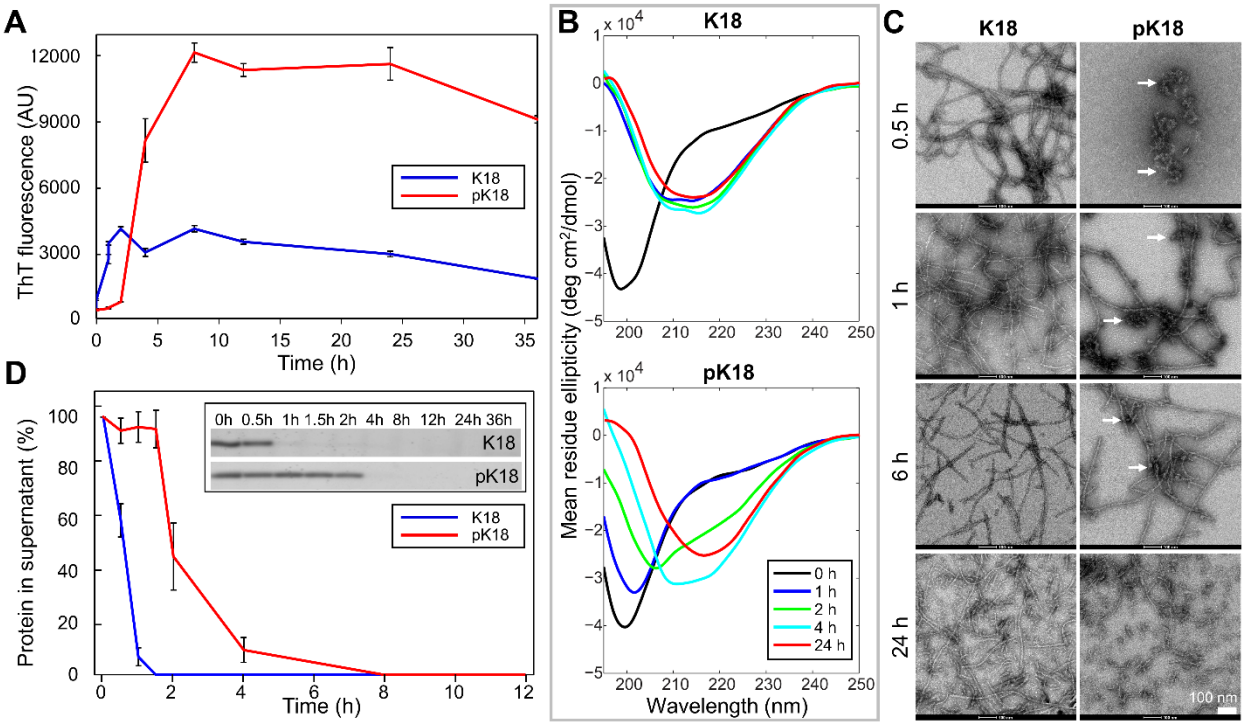

Figure 6. Aggregation behavior of non-phosphorylated K18 compared to phosphorylated pK18. 10 µM K18 and pK18 were incubated for several days at 37°C under shaking conditions, in the presence of 2.5 µM heparin. **(A)** ThT fluorescence was measured at different time points and reported as a ThT kinetics (graph showing one representative example). K18 reached a plateau after about 2 h, while pK18 presented a longer lag phase and reached a plateau only after 7 h of incubation. However, the pK18 plateau intensity was around three times higher than that of the K18 protein. (**B)** At several times points, an aliquot of the aggregation reaction was taken and centrifuged. The supernatants were run on an SDS−PAGE (inlet). The supernatant band intensity from four independent experiments was quantified and reported as the percent of protein remaining in the supernatant (mean +/S.E.M). pK18 required more time (4 h) to become fully insoluble compared to 1 h for K18. **(C)** CD spectra recorded at different time points showed that the K18 protein fully converted into β−sheet-containing species after 1 h, while the pK18 became β−sheet−rich only after 4 h. **(D)** Electron micrographs of the samples at several time points. While K18 showed fully formed fibrils after 0.5 h, the pK18 first formed protofibril−like aggregates that became fibrillar after 2 h..

Phosphorylation on tyrosine residues reduces Tau affinity for MTs.

In light of the prominent direct association of Tau with MTs, we next asked whether Tau tyrosine phosphorylation, especially on residues Y310 and Y394, had an effect on Tau microtubule-binding propensity. To address this question, we used full-length Tau phosphorylated by c−Abl, taking advantage of the preferential phosphorylation of Y310 and Y394 among other residues, as demonstrated by mass spectrometry SP counts (Figure 2, D). We first compared the MT-binding properties of Tau and pTau by comparing Tau MT-binding through ratio of bound Tau to free Tau in the MT-binding curve assay (Fig. 7, A). We determined the values of the equilibrium dissociation constant (KD), the maximum binding (Bmax) and the stoichiometry (n) as described in Materials and Methods. We obtained a KD of 0.74 µM for non-phosphorylated Tau, and 1.32 (according to the figure) µM for the pTau. Similarly, we found Bmax = 3.67 µM for Tau and a lower value of 3.04 µM for pTau, and finally n = 0.18 for non-phosphorylated Tau and n = 0.15 for pTau. These data indicate that that the binding affinity for MTs was lower for pTau compared to Tau.

We also assessed the binding propensity of pTau to the MTs by quantifying the percent of protein pelleted when incubated with pre−formed paclitaxel−stabilized MTs at a single concentration (250 µg/ml Tau and 100 µg/ml of tubulin). We observed, as previously reported (16), that Tau bound to tubulin with about 50% efficiency, while this efficiency was decreased to approximately 30% in the case of pTau. As a negative control, the BSA was found to bind MTs with a low efficiency of 12%, and as a positive control, the Microtubule−Associated Protein Fraction (MAPF) showed a high binding of 78% (Fig. 7 B, E), as expected. These results were further confirmed by the SDS-PAGE, where bands corresponding to non-phosphorylated Tau was clearly enriched in the pellet fraction, whereas pTau remained predominantly in the soluble fraction. EM data showed no morphological differences between Tau and pTau-bound MTs (Fig. 7, C).

Our results confirm the negative impact of tyrosine phosphorylation on the interaction of Tau with MTs, likely mediated by the large shift towards the negative electrostatic potential as well as structural rearrangements of MT-binding region through the phosphorylation of C-terminal tyrosine residues Y310 and Y394, with a possible contribution from other phosphorylated tyrosine residues requiring further investigation.

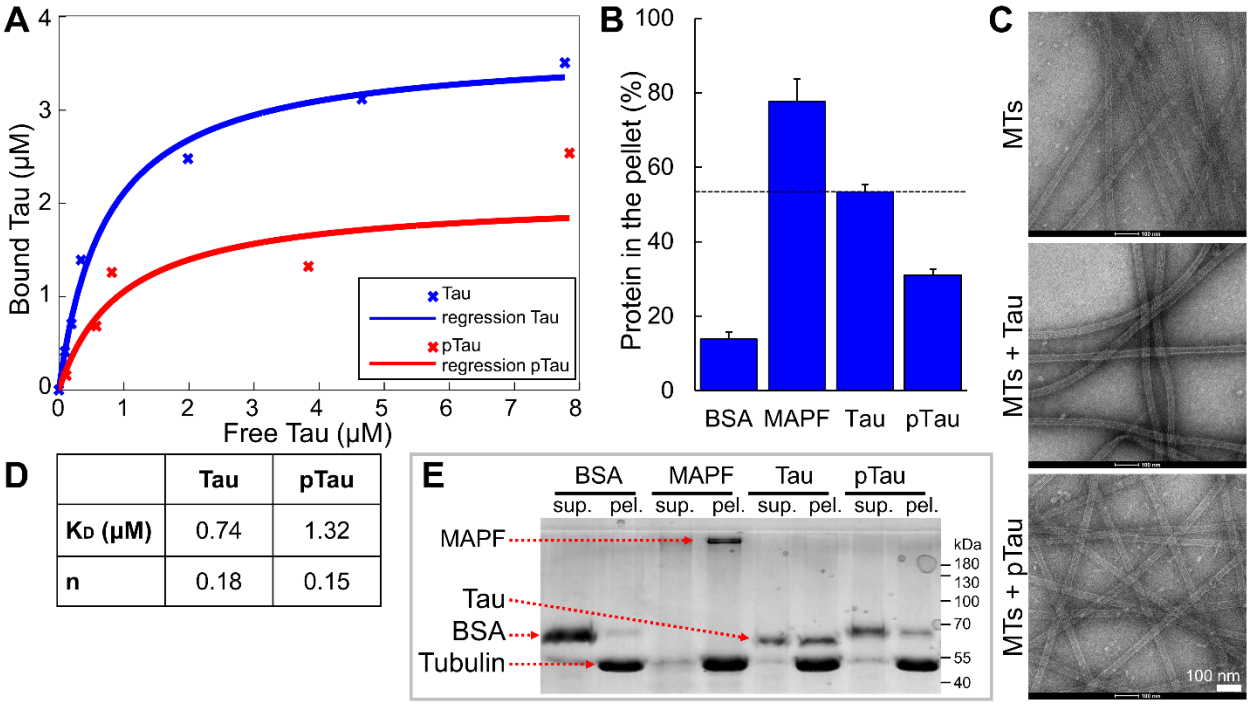

	Tau	pTau
K_D (μM)	0.74	1.32
n	0.18	0.15

Figure 7. Tau/microtubule binding assay. **(A)** MT-binding curves of Tau and pTau. Tau and pTau at concentrations ranging from 0.5 μM to 15 μM bound to pre−formed paclitaxel-stabilized MTs at 4 mg/ml in presence of GTP for 10 min, after which the samples were centrifuged for 40 min at 50 000 g. Western blot analysis was performed to determine the amount of bound Tau (i.e. co−pelleted with the tubulin), and the free Tau (remaining in the supernatant). The binding curves were generated by plotting bound versus free fractions (corrected for their initial concentration, each data point was represented as a dot on the graph), and the data were fitted using non−linear regression to the standard binding equation for a macromolecule (i.e. MTs) containing equivalent and non−interacting ligand (i.e. Tau) binding sites: Tau on the graph). **(B)** The binding propensity of pTau to the MTs was quantified as the percent of protein pelleted when incubated with pre−formed paclitaxel−stabilized MTs at a single concentration (250 μg/ml pTau and 100 μg/ml of tubulin). The averaged quantification from 5 repeats, represented as mean +/S.E.M. **(C)** EM micrographs of paclitaxel−stabilized MTs alone and incubated with Tau or pTau. **(D)** For the non−linear regression, the following parameters were obtained: equilibrium dissociation constant KD, maximum binding Bmax and stoichiometry n, which was found through the relationship Bmas = n * [tubulin dimers]. **(E)** Representative SDS-PAGE showed that Tau bound to tubulin with about 50 % efficiency, while this efficiency was decreased to about 30 % in the case of pTau. As a negative control, the BSA was found to bind MTs with a low efficiency of 12%, and as a positive control, the Microtubule−Associated Protein Fraction (MAPF) showed a high binding of 78%. E, EM micrographs of paclitaxel−stabilized MTs alone and incubated with Tau or pTau. The MTs were formed as expected and there were no obvious differences in MTs morphology in presence of Tau or pTau.

Phosphorylation on tyrosine residues reduces Tau affinity for and binding of lipid vesicles.

We have previously shown that both Tau and K18 interact with brain phosphatidylserine (BPS) vesicles resulting in vesicle disruption and the formation of highly stable oligomeric protein/phospholipid complexes (48). Therefore, we sought to assess whether phosphorylation on tyrosine residues influenced Tau interaction with membranous vesicles and the formation of such Tau-phospholipid complexes.

To address this question, we incubated Tau and K18 and their respective tyrosine-phosphorylated forms with BPS vesicles at a molar Tau to phospholipid ratio of 1 to 1 and performed sedimentation assay. We found that Tau and K18 incubated with BPS vesicles co−sedimented with vesicles to a larger extent than with their phosphorylated counterparts. This is demonstrated by the reduction of phosphorylated Tau and K18 in the pellet fractions (Fig. 8, A, red box), signifying reduced Tau affinity and binding of the lipids.

Next, to confirm the formation of oligomeric Tau- and K18-phospholipid complexes, Native gel analysis was performed, and showed the formation of oligomeric species by both non-phosphorylated and phosphorylated Tau and K18 (Fig. 8, B, red boxes). These findings were further supported by the EM data, where oligomeric complexes were detected for all proteins without discernible morphological differences (Fig. 8, C), indicating no differences in the absolute capacity of pTau and pK18 to form oligomeric structures compared to their non-phosphorylated counterparts.

Next, to verify the formation of the Tau/K18 phospholipid-oligomer complexes by the non-phosphorylated and phosphorylated Tau and K18, size exclusion chromatography (SEC) was performed. pTau and pK18 complexes peaks (Fig. 8, E, red) systematically eluted later compared to their non-phosphorylated counterparts (Fig. 8, E, blue; dashed lines indicate peaks of the elution profiles, arrows indicate the direction of elution profile shift), closer to the elution of profile of monomeric phosphorylated Tau and K18 variants in the absence of BPS (Fig. 8, E, dashed). These data are well in line with biochemical data (Fig. 8, A, B) and suggest that Tau-lipid complex formation is affected by tyrosine phosphorylation of Tau and K18, resulting in smaller oligomeric Tau- and K18-phospholipid complexes on average, either through the reduction of the number of protein and/or phospholipid molecules per complex, through complex compaction or reduced stability.

Tau and K18 were reported to undergo the structural transitions upon binding to lipid membranes (49-52). Therefore, to elucidate the conformational effects of phospholipids on tyrosine-phosphorylated Tau and K18, we monitored changes in Tau and K18 secondary structures by CD spectroscopy. Interestingly, the conformational transitions in the presence of BPS vesicles were markedly more pronounced for non-phosphorylated Tau and K18, with curves indicating a mixture of structural conformers, compared to pTau and pK18 (Fig. 8, D), in correspondence to less pronounced structural conformation transitions during the aggregation reactions (see Fig. 3, B). As CD spectroscopy reports the average structure within the mixture, it is possible, however, that non-lipid-bound phosphorylated Tau and K18 predominate the conformational landscape at any given moment in time.

Our results demonstrate that phosphorylated Tau and K18 had reduced lipid vesicle binding affinity and formed oligomers that showed less pronounced structural conformation transitions and SEC elution profiles, and that were shifted towards smaller species compared to non-phosphorylated Tau and K18 in the presence of BPS vesicles. However, the capacity to associate with lipids was still preserved in the phosphorylated variants.

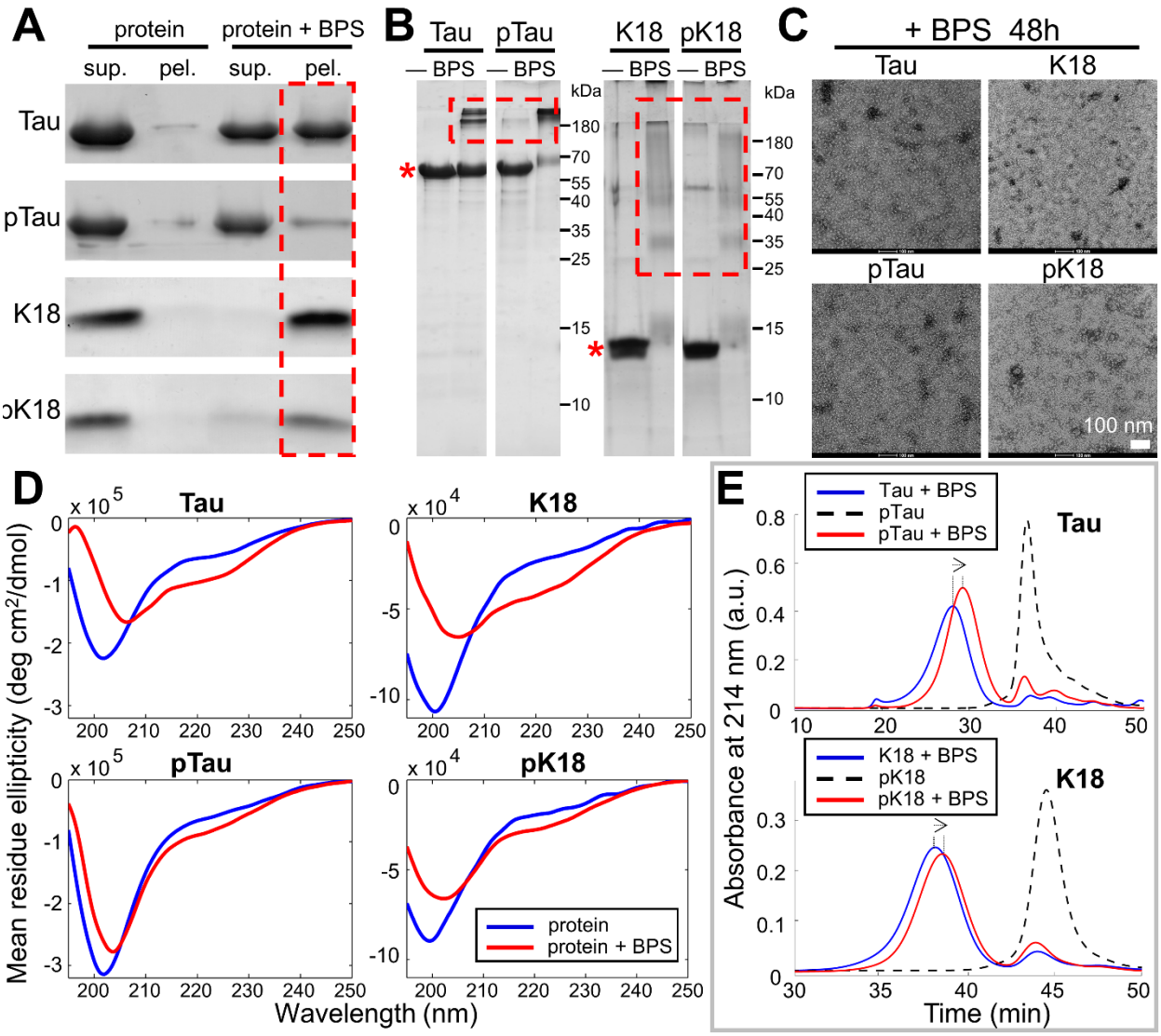

Figure 8. Lipid binding behavior of pTau and pK18. Co−sedimentation assay of BPS vesicles with 10 µM Tau, K18, pTau and pK18 at a molar ratio 1:20 (protein:phospholipid). **(A)** When incubated alone (left), all proteins remained in the supernatant (sup.), but in the presence of BPS vesicles (right) proteins partially co−sedimented with the vesicles in the pellet fraction (pel.), indicating membrane binding (dashed red rectangle). **(B)** CD spectra of Tau (left top panel), K18 (right top panel), pTau (left bottom panel), pK18 (right bottom panel) alone (blue) and in presence of BPS vesicles at a molar protein:phospholipid ratio of 1:20 (red). **(C)** Native PAGE analysis of protein/phospholipid complexes formed by Tau, pTau (left) and K18, pK18 (right) after 24 h of incubation with BPS vesicles at a molar protein:phospholipid ratio of 1:20. The monomer bands are indicated by asterisks and the presence of higher molecular weight bands indicated by red dashed rectangles demonstrates that the complexes contain oligomerized proteins. **(D)** Corresponding EM micrographs show that both WT and phosphorylated proteins were able to form phospholipid/protein complexes. **(E)** Top panel: size−exclusion chromatograms of Tau (blue line) and pTau (red line) incubated in the presence of BPS at molar ratio 1:20 (protein:phospholipid) or alone (dashed line). Bottom panel: size−exclusion chromatograms of WT K18 (blue line), pK18 (red line) incubated in the presence of BPS at molar ratio 1:20 (protein:phospholipid) or alone (dashed line). Dotted lines demarcate the elution peaks, arrows show the direction of the peak shift.

Tyrosine 310 phosphorylation underlies the structural basis of the lowered Tau affinity for and binding of lipid vesicles.

Next, we sought to determine the underlying structural basis for the reduced lipid-binding affinity of tyrosine-phosphorylated Tau. Previously, we showed that the core of the highly-stable oligomeric Tau-phospholipid complexes was comprised of both the PHF6* and PHF6 hexapeptide motifs, the latter in a β−sheet conformation. Since the Y310 residue is located in the PHF6 hexapeptide, part of the R3 repeat peptide (Fig. 1), which plays an important role in mediating the interaction between Tau and membranes (48,53), we set out to assess the effect of R3 Y310 phosphorylation on lipid-mediated formation of fibrils by R3 and its interaction with membranes *in vitro*.

First, we incubated R3 and pR3 peptides with BPS vesicles at a molar peptide to phospholipid ratio of 1 to 1 and monitored fibril formation using EM (Fig. 9, A). We observed a rapid formation of large fibrils by R3, whereas the pR3 peptide exhibited a significant delay in fibril formation (Fig. 9, A, 1h). Furthermore, whereas R3 formed long fibrils at a later time point, pR3 formed fibrils relatively shorter than R3 (Fig. 9, A, 24h, insets).

Next, we observed the direct incorporation of the phospholipids within the fibrillar R3 matrix and assessed the effects of Y310 phosphorylation of R3 peptide. To this end we co−incubated the R3 and pR3 with vesicles containing 1% NBD−labelled fluorescent phospholipids (fPS). Under these conditions, we observed the formation of fluorescent fibrils in the case of R3, suggesting that R3 bound to and incorporated phospholipids within the fibril matrix. No fluorescent signal was observed in the case of the fibrils formed by pR3, suggesting that they were devoid of phospholipids (Fig. 9, B).

To further confirm the interaction of R3 and pR3 with the phospholipids, we performed a sedimentation assay by incubating R3 and pR3 for 24 h with BPS vesicles containing 1% NBD−labelled fluorescent phospholipids, subsequently centrifuged, and run on SDS−PAGE imaged with a fluorescent scanner (Fig. 9, C). In this assay, vesicles alone floated and did not pellet. We observed that phospholipids in the R3 sample were solely present in the pellet fraction after 24 h incubation, but that only a small fraction of the phospholipids in the pR3 sample were found in the pellet (Fig. 9, D). These results further confirm our EM and fluorescence microscopy data and indicate that the capacity of R3 to form fibrils that contain

phospholipids in the presence of BPS vesicles was significantly diminished by phosphorylation of residue Y310.

These findings are in line with data obtained with the full-length Tau and K18 data (Fig. 8), and further suggest that lipid incorporation into fibrillar matrix is mediated by the aggregation−prone PHF6 peptide in R3, and that phosphorylation at Y310 residue in the R3 peptide underlies the structural basis for the diminished interactions with negatively charged vesicles.

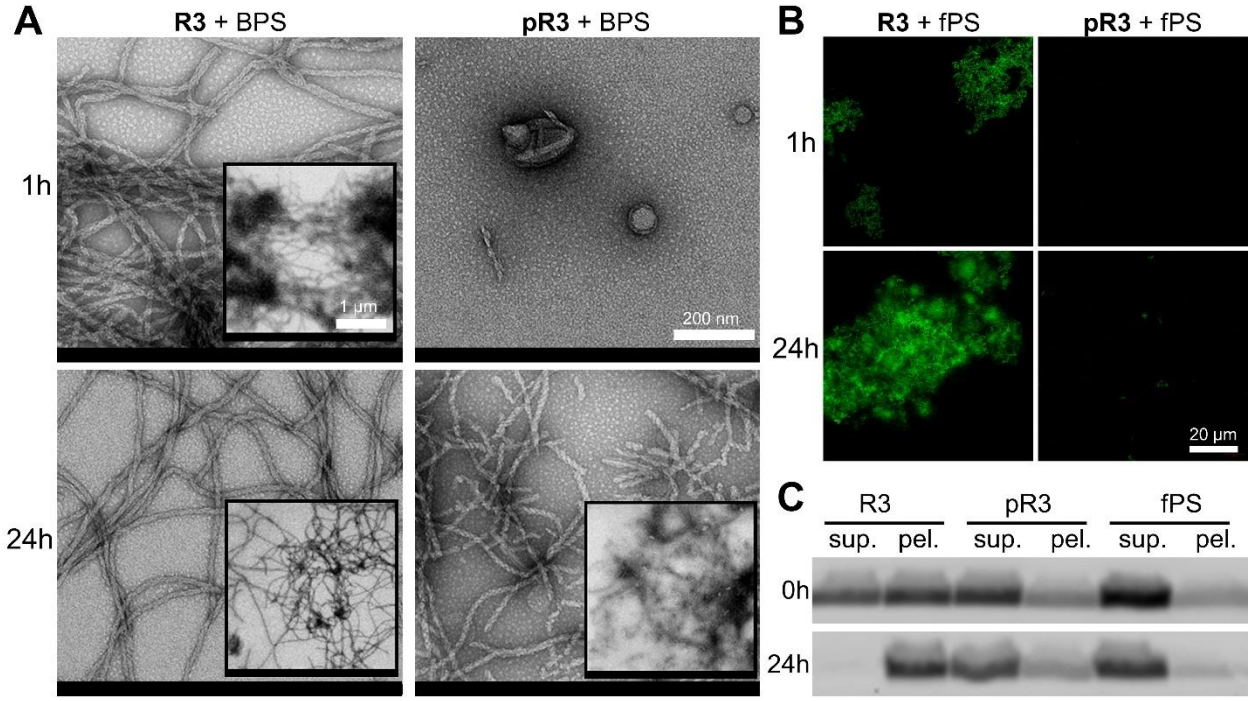

Figure 9. Lipid binding propensity of non-phosphorylated R3 compared to phosphorylated pR3 peptides. **(A)** EM and **(B)** fluorescence microscopy images of 100 µM R3 and pR3 peptides incubated for 1 h, 1 day or 2 days with BPS vesicles at a molar ratio of 1:1. For fluorescence microscopy, R3 or pR3 peptides were incubated with vesicles containing 1% fluorescent NBD−labeled phospholipids (fPS). **(C)** SDS−PAGE gel analysis of the sedimentation assays.

DISCUSSION

Despite the presence of tyrosine residues in domains that regulate Tau interactions with microtubules and its aggregation propensity, the role of Tau tyrosine phosphorylation in regulating Tau functions, structure, aggregation and toxicity remain generally understudied. For example, tyrosine 310 residue is located in the PHF6 motif of Tau protein, which has been identified as forming β-sheet structure in the core of Tau fibrils and is necessary for Tau aggregation. Despite consistent findings implicating PHF6 in the initiation of Tau aggregation, stabilization of Tau fibrils and the importance of the interaction of Y310 and I308 for Tau filament formation (29), there are no reports in the literature examining the potential impact of phosphorylation at this residue on the physiological and/or pathogenic properties of biologically-relevant full-length Tau proteoforms, possibly due to the lack of well-characterised antibodies targeting PTMs in this domain.

Due to the prominent position of Y310 within the aggregation-prone PHF6 motif of the Tau MT-binding domain, we speculated that modifications, such as the addition of bulky negatively-charged phospho-group to Y310 in the context of full-length Tau may play key roles in impacting the structural and biophysical characteristics of biologically-relevant Tau proteoforms and influence Tau aggregation. In addition, stoichiometry and localization of Tau tyrosine post-translational modifications may confer differential effects on either N-terminal domain (Y18, Y29), that is implicated in Tau secretion (54) and regulation of microtubule stabilization (55), or on mid– and C-terminal domains (Y197, Y310, Y394), that are implicated in modulation of Tau aggregation, microtubule- and lipid-binding properties (for a recent review see (56)) of Tau molecule. Furthermore, recent studies using cryoelectron microscopy of Tau filaments from human brain confirmed the PHF6 motif as a core component of Tau filaments, with Y310 buried within the interior of Tau filament in Pick's disease, as well as in PHFs and SFs in AD, and Tau filaments in CTE (57-59) (Figure 10), supporting our initial rationale for investigation.

Our results indicate that a) phosphorylation of Tau at multiple tyrosine residues inhibits Tau aggregation through cumulative effects of phosphorylation at all tyrosine residues, and that b) phosphorylation at residue Y310 is a key determinant of Tau aggregation *in vitro.* We show that Y310 phosphorylation appears to be sufficient to suppress or significantly delay Tau aggregation. On the other hand, our data strongly indicate that phosphorylation at residue Y310 also reduces the propensity of the microtubule-binding region of Tau to aggregate through attenuation of the PHF6 hexapeptide propensity to adopt β-sheet rich structure in the

context of the full-length Tau. Structural studies by NMR revealed that phosphorylation at Y310 induced local structural modifications in the PHF6 region of K18, thereby decreasing its propensity to adopt a β-sheet-containing secondary structure, contributing to the decreased aggregation propensity.

Y310 is the only tyrosine residue located in the MT-binding region of Tau, which highlights the potential role of Y310 in regulating Tau affinity for MTs. Our work shows that phosphorylation on tyrosine residues affects full-length Tau affinity for MTs, in contrast to previous reports where Tau phosphorylated by Fyn (16), Arg (19) or c-Abl (18) *in vitro* was found to bind to MTs with an efficiency similar to that of the non-phosphorylated protein. These findings suggest that tyrosine phosphorylation of Tau on either Y18 (i.e. by Fyn) or Y394 (by c-Abl or Arg) did not significantly alter its affinity for MTs. Our data point toward residue Y310 as an important regulator of Tau/MTs interactions, as pTau used in our study was mainly phosphorylated at residues Y310 and Y394 (Figure 2, D). Here we present the first report implicating the importance of tyrosine phosphorylation in the MT-binding domain of Tau and argue for a role of tyrosine kinases targeting of Tau residue Y310 in the regulation of cytoskeleton dynamics.

The fact that MT-binding domain of Tau is also responsible for Tau-lipid interactions points to the potential role of Y310 in regulating Tau affinity for lipid membranes. We have previously demonstrated that the PHF6 hexapeptide located within R3 interacted with negatively charged vesicles, resulting in the formation of β−strand—rich mixed phospholipid/peptide fibrils (48). In this work, we show that tyrosine phosphorylation, at least at residue Y310, diminished Tau binding to negatively-charged lipid membranes, which may have important implications for Tau functions at the cell plasma membrane.

Our findings are especially relevant in the light of reports demonstrating that Tau tyrosine phosphorylation occurs in the human brain under physiological and pathological conditions. Tau amino terminal regions contain several potential SRC homology 3 (SH3) binding motifs (PXXP), which makes it a potential substrate for phosphorylation by SH3 domain-containing cytoplasmic tyrosine kinases.

However, while the aberrant serine and threonine phosphorylation of Tau is well-established in AD (60), specific contributions of tyrosine phosphorylation to Tau-mediated pathology in AD are not fully known. Several lines of evidence suggest that Tau tyrosine phosphorylation is an early event in the development of AD (61). In 1991, Wood and Zinmeister used pan anti-phosphotyrosine antibodies to demonstrate the

increase of non-specific tyrosine phosphorylation in AD patient's brain tissue of NFT-bearing neuronal somatodendritic and dystrophic neurite compartments, as well as microglia-resembling cells within neuritic plaques, compared to predominantly developing neurite staining of non-AD tissue (62). Similarly, during the same year, Shapiro *et al.* found increased non-specific phosphotyrosine immunoreactivity in the frontal cortex and hippocampus of AD patients (63). Since then, several reports based on antibody recognition or mass spectrometry have shown that Tau is phosphorylated on residues Y18, Y197 and Y394 (16,18,19,64) in AD and in foetal brain, whereas only phosphorylation at position Y394 has been clearly shown to occur under physiological conditions (18). Furthermore, in the P301L transgenic mouse model, Vega *et al.* showed that Tau phosphorylation at residues Y197 and Y394 correlated with the formation of Tau aggregates and occurred concurrently with serine and threonine phosphorylation (detected by PHF1 antibody at residues S396/S404 and by CP13 at residues S202/T205) known to be implicated in AD pathogenesis (64). Moreover, two tyrosine kinases, Fyn and c-Abl have been shown to co-localize with Tau in NFTs (18,65), and treatment with Aβ resulted in an increase in the activity of both kinases and led to subsequent increase in Tau tyrosine phosphorylation and cell death, which could be prevented by treatment with tyrosine kinase inhibitors (66). In addition, Tau tyrosine phosphorylation may be involved in regulating several cellular activities of Tau linked to signalling events at the cell membrane, in lipid rafts and/or in the neuron growth cone (16,18). Overall, these findings strongly suggest that Tau tyrosine phosphorylation plays important roles in both the healthy state and in neurodegenerative disease conditions (67), and further studies investigating the specific role of Tau residue Y310 modifications are warranted.

In conclusion, our findings show that Tau phosphorylation on five tyrosine residues may have synergistic effects on Tau fibril formation, MT- and lipid-binding affinity based on stoichiometry and localization of PTMs. In addition, our findings underscore the unique role of Y310 phosphorylation, which is consistent with its position within the aggregation-prone PHF6 hexapeptide, itself located in the MT-binding domain of the protein. We show that phosphorylation at Y310 is sufficient to significantly delay the fibrillization of full-length Tau and K18, and of the R3 repeat fragment. Our results strongly implicate tyrosine phosphorylation of Tau as a novel target for disease-modifying therapies of proteopathic disorders featuring Tau aggregation. Furthermore, our results underscore the critical importance of developing the right tools to assess the extent of Tau tyrosine phosphorylation in different Tauopathies and enable investigations of the role of phosphorylation in regulating Tau function in health and disease.

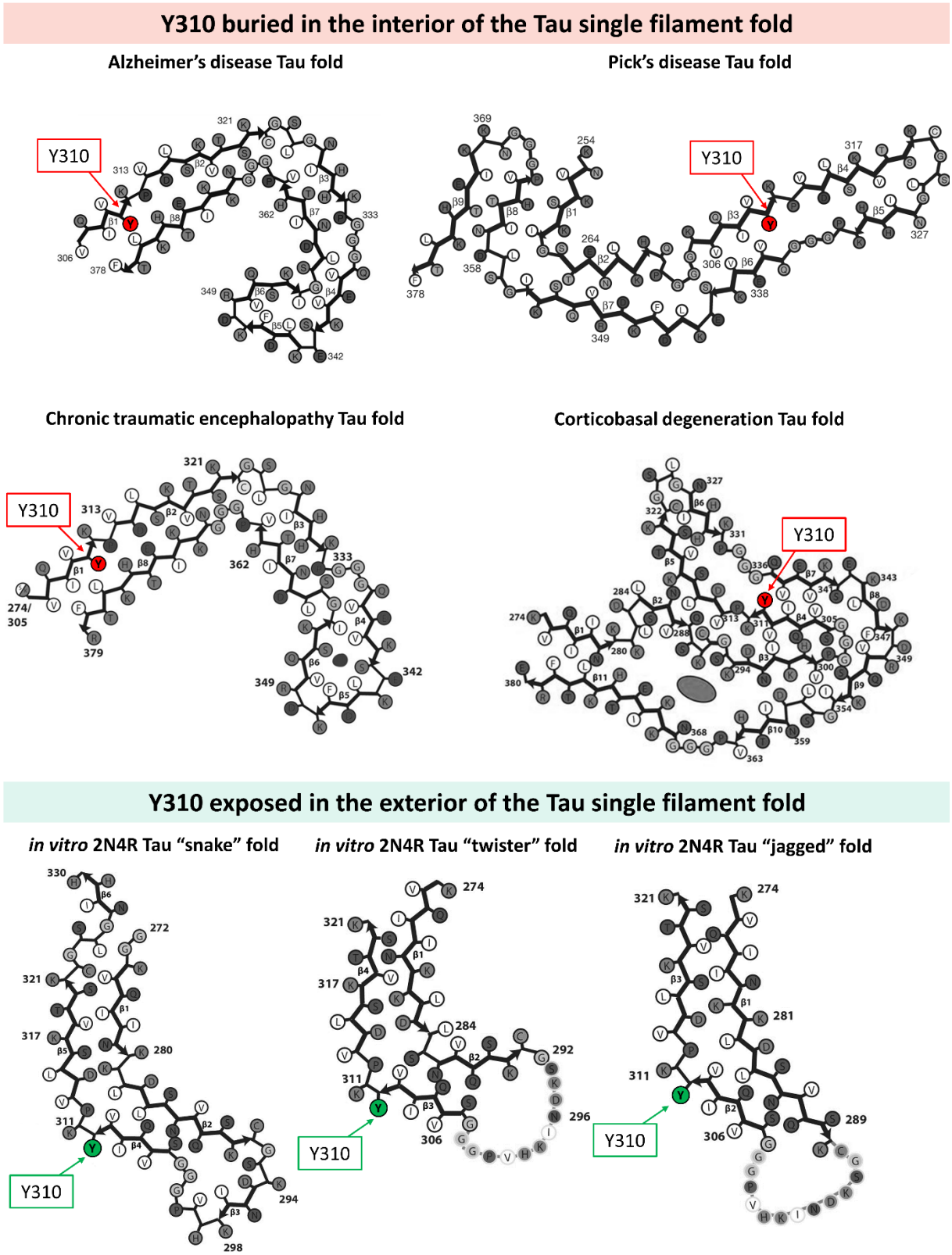

Figure 10. Schematic representations of Tau filament core fold. Y310 residue is buried in the interior (red) of the Tau single filament fold in structures derived from AD, PiD, CTE and CBD-Tau, or exposed in the exterior (green) in *in vitro*-derived Tau structures. Adapted from (57-59,75,76).

EXPERIMENTAL PROCEDURES

DNA constructs and mutagenesis. The K18 fragments were synthesized by GeneArt Gene Synthesis (Life Technologies) and cloned into the pT7-7 for bacterial expression. Tau 2N4R in pCMV6-XL5 vectors was obtained from OriGene Technologies, Inc. and cloned in pET-15b for bacterial expression. Single site mutagenesis was performed in the pET-15b using the QuikChange Site-Directed Mutagenesis Kit (Stratagene), as per manufacturer's instructions. pET21d SH2-CD c-abl T231R and pCDFDuet-1 YopH for bacterial expression were kindly donated by Prof. Oliver Hantschel (ISREC Institute, EPFL).

Peptides. The R3 (306-VQIVYKPVDLSKVTSKCGSLGNIHHK-331and the pY-R3 (306-VQIV(pY)KPVDLSKVTSKCGSLGNIHHK-331) corresponding to the third microtubule-binding repeat without/with phosphorylation at Y310 were purchased from CS Bio Co.

Other compounds. Tubulin protein isolated from porcine brain (97% or >99 % pure), provided as a lyophilized powder was purchased from Cytoskeleton Inc. Paclitaxel from the pacific yew tree, *Taxus brevifolia* (purity of >99.5%), used inhibit microtubule depolymerization, provided as a lyophilized powder and resuspended at 2 mM anhydrous DMSO was purchased from Cytoskeleton Inc. (U.S.A). Guanosine triphosphate (GTP) provided as a lyophilized powder, resolubilized at 100 mM with ice-cold MilliQ water was purchased from Cytoskeleton Inc. (U.S.A). Microtubule (MT) associated protein fraction (MAPF) isolated from bovine brain, used as positive control for the MT binding assay, supplied as lyophilized powder was purchased from Cytoskeleton Inc. (U.S.A). Phosphatidylserine isolated from porcine brain (BPS) and fluorescently labeled phospholipid 1-oleoyl-2-{6-[(7-nitro-2-1,3-benzoxadiazol-4-yl)amino]hexanoylM-sn-glycero-3-phosphoserine (fPS) were purchased from Avanti Polar Lipids, Inc.. Heparin sodium salt was from Applichem GmbH.

Protein expression and purification (Tau and K18). Tau isoforms 2N4R in pET-15b, K18 in pT7-7 were expressed in E. coli strain BL21. The purification protocol of Tau 2N4R Tau was adapted from (68). Cells were pelleted and broken by sonication in lysis buffer (3 M urea in 10 mM MES, pH 6.5, 1 mM DTT, 1 mM EDTA, 1 mM PMSF). After centrifugation at 150,000 g for 1 h at 4°C, 1% (w/v) of streptomycin sulfate was added to the supernatant, and the solution was stirred for 90 min at 4°C. After centrifugation at 27,000 g for 1 h at 4°C, the supernatant was dialyzed overnight at 4°C in ion exchange (IEX) buffer A (10 mM MES, pH 6.5, 20 mM NaCl, 1 mM DTT, 1 mM EDTA). The supernatant was filtered and loaded on a

cation-exchange column (MonoS, GE Healthcare) and the protein was eluted using a salt gradient (increasing the NaCl concentration of IEX buffer A from 20 mM to 1 M NaCl over 20 column volumes). Fractions containing the proteins were dialyzed overnight against acetic buffer (5% acetic acid in water) and loaded on a reverse-phase HPLC C4 column (PROTO 300 C4 10 µm, Higgins Analytical; buffer A: 0.1% TFA in water, buffer B: 0.1% TFA in acetonitrile), and the protein was eluted using a gradient from 30 to 40% buffer B over 40 min (15 ml/min). K18 in pT7-7 was purified following a protocol adapted from (69). Briefly, cells were broken by sonication in IEX buffer B (10 mM HEPES, pH 6.5, 1 mM MgCl2, 20 mM NaCl, 1 mM DTT, 1 mM PMSF). After centrifugation at 40,000 g for 30 min, the supernatant was boiled until the solution became cloudy (~5 min) and centrifuged again for 30 min. The supernatant was filtered and loaded on a cation-exchange column (MonoS, GE Healthcare), and the protein was eluted using a salt gradient (increasing the NaCl concentration of IEX buffer B from 20 mM to 1 M NaCl over 20 column volumes). Fractions containing the K18 fragment were immediately loaded on a reverse-phase HPLC C4 column (PROTO 300 C4 10 µm, Higgins Analytical; buffer A: 0.1% TFA in water, buffer B: 0.1% TFA in acetonitrile), and the protein was eluted using a gradient from 30 to 40% buffer B over 40 min (15 ml/min).

SH2-CD c-Abl expression and purification. Recombinant SH2-CD c-Abl, T231R and YopH were co-overexpressed and SH2-CD c-Abl purified from E.coli as previously described (70). Briefly, cells were grown in 2 L of TB media, until the OD reached 1.0, after which the cultures were cooled down and induced overnight at 18°C, with 0.2 mM IPTG. The cells were then lysed by sonication in HisTag binding buffer HA (50 mM Tris pH 8, 500 mM NaCl, 5% Glycerol, 25 mM imidazole) and centrifuged twice at high speed (50 000 g, 20 min, 4°C), before being injected in 5 mL HisTag columns (histrap 5mL column, GE Healthcare, buffer HA: same as above, buffer HB: same as HA with 0.5 M imidazole). Selected fractions were desalted using two HiPrep 26/10 desalting columns (GE Healthcare) in series (Desalting buffer: 20 mM Tris pH 8, 50 mM NaCl, 5 % Glycerol, 1 mM DTT), combined and further purified by anion-exchange chromatography using a MonoQ 5/50 GL column (GE Healthcare, buffer A: 20 mM Tris, 5% Glycerol, 1 mM DTT, pH 8.0, buffer B: same as buffer A with 1 M NaCl). The final concentration of the c-Abl kinase was determined using the UV absorbance at 280 nm (M = 46797 g.mol-1 and ε280 = 80010 M-1.cm-1).

Large scale Preparation of phosphorylated K18, Tau and Y-> F mutants by c-Abl. The large scale phosphorylation of 10 mg K18, Tau and Tau Y-> F mutants were performed for 4 h in 50 mM Tris, 5 mM MgCl2, 1 mM DTT, 20 mM Na3VO4 (phosphatase inhibitor) in the presence of 3 mM MgATP, pH,7.5 at 30°C. We used c-Abl kinase at a ratio of 1:20 (kinase:Tau). The reaction mixture was followed by ESI-MS

to verify the completion of the phosphorylation. Additional kinase and MgATP were added when needed. Phosphorylated K18, Tau and Y-> F mutants were purified by reverse-phase HPLC preparative C4 column (PROTO 300 C4 10 µm Higgins Analytical; buffer A: 0.1% TFA in water, buffer B: 0.1% TFA in acetonitrile) using a linear gradient of 30 to 40 % of B in 40 min for Tau or 20 to 35 % of B in 40 min for K18. The HPLC fractions were analyzed ny LC-MS and the Pure once were pooled and lyophilized.

Preparation and characterization of heparin-induced Tau and K18 fibrils. Fibrils of WT, mutants and phosphorylated Tau and K18 were formed by incubating monomeric protein in 10 mM phosphate, pH 7.4, 50 mM NaF and 0.5 mM DTT with heparin sodium salt (Applichem GmbH) at a molar heparin:protein ratio of 1:4 under constant orbital agitation (1000 rpm, Peqlab, Thriller) at 37°C for up to 72 hours.

R3 and pY-R3 peptide aggregation. 100 µM R3 or pY-R3 peptide were dissolved in 10 mM Tris, 50 mM NaF,0.5 mM DTT and pH-adjusted to 7.4. The solution was then vortexed, centrifuged for 20 min at 14000 rpm and the supernatant was incubated in absence or presence of 25 µM heparin sodium salt (Ap-plichem GmbH) at 37 °C, with constant orbital agitation (1000 rpm, Peqlab, Thriller).

Vesicle preparations. Vesicles were prepared using the extrusion method. Briefly, individual phospholipids or phospholipid mixtures in chloroform were dried using an argon stream to form a thin film on the wall of a glass vial. Potentially remaining chloroform was removed by placing the vial under vacuum overnight. The phospholipids were resolubilized in 10 mM HEPES, pH 7.4, 100 mM NaCl and 2.5 mM DTT to the desired final concentration by sonication. The solution was then passed through an Avestin LiposoFast extruder (Avestin Inc.) (membrane pore size: 0.1 µM), and the size and homogeneity of the resulting vesicles were assessed by TEM. For the preparation of fluorescently labeled vesicles, fluorescent and non-fluorescent phospholipids in chloroform were mixed at a molar ratio of 1:99 prior to the initial drying step.

Preparation of mixed protein/phospholipid complexes. Protein/phospholipid complexes were prepared by incubating BPS vesicles with Tau, K18 or α-Syn at a molar protein:phospholipid ratio of 1:20 in 10 mM HEPES, pH 7.4, 100 mM NaCl, 2.5 mM DTT for 48 h at 37°C. The resulting protein/phospholipid complexes were separated from the remaining vesicles and soluble protein by SEC using a Superose 6 column (GE Healthcare).

Preparation of mixed R3 and pY-R3 peptides/phospholipid fibrils. 100 µM of R3 and pY-R3 peptides were incubated with BPS vesicles at a molar ratio of 1:1. For fluorescence microscopy, the peptides were incubated with vesicles containing 1% fluorescent NBD-phospholipids, imaged with confocal laser-scanning microscope (LSM 700, Zeiss) and analyzed using Zen software.

Preparation of Microtubules. Tubulin was dissolved at a concentration of 5 mg/ml in ice-cold General tubulin buffer (80 mM PIPES, 0.5 mM EGTA, 2 mM MgCl2, pH 6.9) supplemented with 1 mM GTP and snap-frozen as 10 µl aliquots in liquid nitrogen and stored at -80°C. Microtubules were assembled by defrosting an aliquot of 10 µl tubulin stock in a RT water bath, immediately placed on ice and incubated for 20 min at 35°C in 100 µl pre-warmed (35°C) General tubulin buffer supplemented with 1 mM GTP and 5% glycerol. Then the solution was diluted with 100 µl General tubulin buffer supplemented with 1 µl of paclitaxel (Taxol©, stock at 2 mM), gently mixed and kept at RT. Microtubule morphology was systematically verified by electron microscopy.

Microtubule binding assay. Pre-formed paclitaxel-stabilized MTs were incubated for 30 min at RT with Tau, pTau, MAPF or bovine serum albumin (BSA) (250 µg/ml protein and 100 µg/ml of tubulin) in General tubulin buffer supplemented with 1 mM GTP and 5% glycerol (total of 50 µl per sample). The samples were placed on top of a 100 µl Cushion buffer (i.e. General tubulin buffer containing 60 % glycerol) in 1.5 ml tubes. The tubes were centrifuged at 100’000 g for 40 min at RT. The top 50 µl of each tube was mixed with 10 µl of 5x Laemmli buffer (supernatant) and the pellet was resuspended in 50 µl 1x Laemmli buffer (pellet). The samples were run on SDS–PAGE gels. The relative amount of Tau, pTau, MAPF or BSA in the supernatant and in the pellet were estimated by measuring the band intensity using Fiji software (National Institute of Health) over 5 repeats, and represented as mean +/- S.E.M.

Microtubule binding curve. Tau and pTau, at concentrations ranging from 0.5 µM to 15 µM, dissolved in General tubulin buffer supplemented with 5 mM DTT were allowed to bind to pre-formed paclitaxel-stabilized MTs at 4 mg/ml in presence of GTP for 10 min at RT, after what the samples were centrifuged for 40 min at 50’000 g at RT. The supernatant and pellets were run on SDS-PAGE and transferred to nitrocellulose membranes transferred onto nitrocellulose membrane (Fisher Scientific) using the Bio-Rad Trans-Blot Turbo Transfer System. The membranes were blocked in Odyssey blocking buffer (Li-Cor Biosciences GmbH) diluted 1:3 in PBS for 1 h at RT and then incubated with the anti-human Tau antibody (Tau13) for 2 h at RT. The membranes were washed three times in PBS + 0.1% Tween (PBST), incubated

for 1 h at RT with fluorescently labelled secondary antibodies, washed 3 times with PBST, after which the membranes were imaged on a Li-Cor Odyssey CLx scanner (Li-Cor Biosciences GmbH) at a wavelength of 700 or 800 nm. The amount of Tau_{bound} (i.e. co-pelleted with the tubulin), and the Tau_{free} (remaining in the supernatant) was quantified by measuring the band intensity using Fiji software (National Institute of Health). The binding curves were generated according to previously published protocols(71-73) by plotting the bound versus the free fractions (corrected for their initial concentration, each data point is represented as a dot on the graph), and the data are fitted using non-linear regression using the *nlinfit* function from Matlab (The MathWorks Inc.) to the standard binding equation for a macromolecule (i.e. MT) containing equivalent and non-interacting ligand (i.e. Tau) binding sites: $Tau_{bound} = B_{max}\frac{Tau_{free}}{K_D+Tau_{free}}$, with K_D the equilibrium dissociation constant and B_{max} the maximum binding, with B_{max} related to the stoichiometry n by the relationship $B_{max} = n \cdot [tubulin\ dimers]$

Monitoring of c-Abl Tau/K18 phosphorylation by mass spectrometry. 100 or 200 µg of WT Tau or K18 were incubated with 5 or 10 µg of recombinant c-Abl in 50 mM Tris, 5 mM MgCl2, 1 mM DTT, 20 mM Na3VO4 (phosphatase inhibitor), 3 mM MgATP at a pH of 7.5. Reactions were performed for 4 h at 30°C without agitation. The reactions were followed using ESI–MS on a Thermo LTQ ion trap system and by Western Blotting, probed with monoclonal mouse anti-human Tau (Tau13), polyclonal rabbit anti-total Tau (total), anti-pY310-Tau (pY310) and anti-pY394 (pY394) primary antibodies.

Tandem MS/MS of in vitro c-Abl phosphorylated recombinant Tau. Tau phosphorylated with C-Abl as described above were run on an SDS-PAGE and stained using Simply Blue Safe Stain (Life Technologies). The bands corresponding to Tau were excised, destained with 50% ethanol in 100 mM ammonium bicarbonate, pH 8.4, and dried. The proteins were digested in gel by covering gel pieces with a trypsin solution (12.5 ng/µl in 50 mM ammonium bicarbonate (pH 8.4), 10 mM calcium chloride) at 37°C overnight. The digested peptides were subjected to TiO2 phosphopeptide enrichment, concentrated to dryness, resuspended in acetonitrile and dried again. After repeating this step, the dried peptides were resuspended in 20 µl of 20% formic acid, and 2% acetonitrile, desalted on C18 OMIX tips (Agilent Technologies), and analyzed by a capillary LC–ESI–MS system (Thermo Scientific LTQ Orbitrap instrument). The collected MS/MS spectra were matched against human and scored using Mascot and Sequest algorithms. The data were then analyzed using Scaffold version 4.0 (Proteome Software, http://www.proteomesoftware.com/).

Transmission electron microscopy. Samples (3.5 µl) were applied onto glow-discharged Formvar/carbon-coated 200-mesh copper grids (Electron Microscopy Sciences) for 1 min. The grids were blotted with filter paper, washed twice with ultrapure water and once with staining solution (uranyl for-mate 0.7% (w/V)), and then stained with uranyl formate for 30 sec. The grids were blotted and dried. Specimens were inspected with a Tecnai Spirit BioTWIN operated at 80 kV and equipped with an LaB6 filament and a 4K x 4K FEI Eagle CCD camera.

Circular dichroism (CD) spectroscopy. CD spectra were recorded on a Jasco J-815 CD spectrometer operated at 20°C. To minimize buffer absorption, the buffer was modified to 10 mM phosphate buffer, pH 7.4, with 50 mM NaF and 0.5 mM DTT. CD spectra were acquired from 195 nm to 250 nm at a scan rate of 50 nm/min and in increments of 0.2 nm. For each sample, five spectra were averaged and smoothed using binomial approximation.

Nuclear Magnetic Resonance (NMR) spectroscopy. ^{1}H-^{15}N HSQC spectra were collected at 25 ºC on a Bruker Avance 600 MHz spectrometer using samples containing 500 µM K18 or pK18 peptide in 10 mM Na_2HPO_4, 100 mM NaCl, 1 mM DTT, 10% D_2O buffer at pH 7.4. Resonance assignments are based on the previously published assignments of the K18 spectrum (60).

Sedimentation assay. Taking advantage of the fact that high-speed centrifugation sediments fibrils but not monomeric or soluble oligomeric species, the sedimentation assay makes it possible to assess the ratio of fibrilized-to-soluble protein. 20 µl of WT Tau, K18 or Y->F mutants aggregation reactions were pelleted by ultracentrifugation at 200’000 g of 2 h at 4°C. The supernatant was mixed with 2x Laemmli buffer and run on 15% SDS-PAGE. When stated, the amount of soluble material was quantified by measuring the band intensity using Fiji software (National Institute of Health) and averaged over at least three independent repeats.

Thioflavin T fluorescence measurements. Thioflavin T (ThT) fluorescence reading (excitation wavelength of 450 nm, emission wavelength of 485 nm) was performed in triplicate with a ThT concentration of 60 µM and a peptide concentration of 60 µM or a protein concentration of 3 µM in 50 mM glycine, pH 8.5, using a Bucher Analyst AD plate reader.

Vesicle binding assay. The co-sedimentation assay was used to assess initial binding of protein to vesicles. Tau or K18 WT, or tyrosine phosphorylated (10 µM) were mixed with BPS vesicles (200 µM) to a total volume of 20 µl and immediately centrifuged at 200,000 g for 2 h at 4°C. At this speed, the vesicles pellet, and protein bound to them co-sediment with the vesicles. Both the supernatant, containing unbound protein, and the resuspended pellet, containing vesicles with bound protein, were run on 15% SDS-PAGE gels.

Lipid/peptide fibrils sedimentation assay. To verify whether the fibrils formed by the peptides in the presence of vesicles take up lipids and/or are bound to lipids, we performed a sedimentation assay. 100 µM of the R3 or pY-R3 were incubated for 0 h or 24 h with BPS vesicles containing 1% NBD-labeled fluorescent phospholipids (fPS) at a molar peptide:phospholipid ratio of 1:1. The samples were centrifuged for 5 min at 5000 g and the pellets and supernatants run on SDS-PAGE gels that were imaged with a Typhoon trio fluorescent scanner (GE Healthcare**).**

ACKNOWLEDGMENTS

We would like to thank Dr. Prof Olivier Hantschel (EPFL) for providing us with the c-Abl kinase plasmid, Romain Hamelin and the proteomic core facility (EPFL) for the MS/MS data acquisition. We also would like to acknowledge the EPFL CIME facility providing access to the EM. We thank Nathalie Jordan and Céline Vocat for their excellent technical support with cloning and protein expression/purification, respectively. Support was provided by NIH grant R37AG019391 to D.E. NMR was performed at the Weill Cornell NMR core facility, supported by NIH grant S10OD016320.

CONFLICT OF INTEREST: The authors declare that they have no conflicts of interest with the contents of this article.

REFERENCES

1. Arima, K., Nakamura, M., Sunohara, N., Nishio, T., Ogawa, M., Hirai, S., Kawai, M., and Ikeda, K. (1999) Immunohistochemical and ultrastructural characterization of neuritic clusters around ghost tangles in the hippocampal formation in progressive supranuclear palsy brains. *Acta Neuropathol* **97**, 565-576
2. Ferrer, I., Santpere, G., and van Leeuwen, F. W. (2008) Argyrophilic grain disease. *Brain* **131**, 1416-1432
3. Delacourte, A., and Defossez, A. (1986) Biochemical characterization of an immune serum which specifically marks neurons in neurofibrillary degeneration in Alzheimer's disease. *Comptes rendus de l'Academie des sciences. Serie III, Sciences de la vie* **303**, 439-444
4. Sergeant, N., Wattez, A., and Delacourte, A. (1999) Neurofibrillary Degeneration in Progressive Supranuclear Palsy and Corticobasal Degeneration. *J Neurochem* **72**, 1243-1249
5. Mailliot, C., Sergeant, N., Bussière, T., Caillet-Boudin, M.-L., Delacourte, A., and Buée, L. (1998) Phosphorylation of specific sets of Tau isoforms reflects different neurofibrillary degeneration processes. *FEBS Letters* **433**, 201-204
6. Omalu, B. I., DeKosky, S. T., Minster, R. L., Kamboh, M. I., Hamilton, R. L., and Wecht, C. H. (2005) Chronic Traumatic Encephalopathy in a National Football League Player. *Neurosurgery* **57**, 128-134
7. Vermersch, P., Bordet, R., Ledoze, F., Ruchoux, M.-M., Chapon, F., Thomas, P., Destée, A., Lechevallier, B., and Delacourte, A. (1995) Demonstration of a specific profile of pathological Tau proteins in frontotemporal dementia cases. *Comptes rendus de l'Academie des sciences. Serie III, Sciences de la vie* **318**, 439-445
8. Goedert, M., Spillantini, M. G., Jakes, R., Rutherford, D., and Crowther, R. A. (1989) Multiple isoforms of human microtubule-associated protein Tau: sequences and localization in neurofibrillary tangles of Alzheimer's disease. *Neuron* **3**, 519-526
9. Ercan, E., Eid, S., Weber, C., Kowalski, A., Bichmann, M., Behrendt, A., Matthes, F., Krauss, S., Reinhardt, P., Fulle, S., and Ehrnhoefer, D. E. (2017) A validated antibody panel for the characterization of Tau post-translational modifications. *Molecular Neurodegeneration* **12**
10. Grundke-Iqbal, I., Iqbal, K., Tung, Y. C., Quinlan, M., Wisniewski, H. M., and Binder, L. I. (1986) Abnormal phosphorylation of the microtubule-associated protein Tau (Tau) in Alzheimer cytoskeletal pathology. *Proceedings of the National Academy of Sciences* **83**, 4913-4917
11. Wang, J. Z., Grundke-Iqbal, I., and Iqbal, K. (2007) Kinases and phosphatases and Tau sites involved in Alzheimer neurofibrillary degeneration. *Eur J Neurosci* **25**, 59-68

12. Morishima-Kawashima, M., Hasegawa, M., Takio, K., Suzuki, M., Yoshida, H., Watanabe, A., Titani, K., and Ihara, Y. (1995) Hyperphosphorylation of Tau in PHF. *Neurobiology of Aging* **16**, 365-371

13. Köpke, E., Tung, Y.-C., Shaikh, S., Alonso, A. d. C., Iqbal, K., and Grundke-Iqbal, I. (1993) Microtubule-associated protein Tau. Abnormal phosphorylation of a non-paired helical filament pool in Alzheimer disease. *Journal of Biological Chemistry* **268**, 24374-24384

14. Ksiezakreding, H., Liu, W. K., and Yen, S. H. (1992) Phosphate Analysis and Dephosphorylation of Modified Tau Associated with Paired Helical Filaments. *Brain Res* **597**, 209-219

15. Bancher, C., Brunner, C., Lassmann, H., Budka, H., Jellinger, K., Wiche, G., Seitelberger, F., Grundkeiqbal, I., Iqbal, K., and Wisniewski, H. M. (1989) Accumulation of Abnormally Phosphorylated-Tau Precedes the Formation of Neurofibrillary Tangles in Alzheimers-Disease. *Brain Res* **477**, 90-99

16. Lee, G., Thangavel, R., Sharma, V. M., Litersky, J. M., Bhaskar, K., Fang, S. M., Do, L. H., Andreadis, A., Van Hoesen, G., and Ksiezak-Reding, H. (2004) Phosphorylation of Tau by fyn: Implications for Alzheimer's disease. *J Neurosci* **24**, 2304-2312

17. Scales, T. M. E., Derkinderen, P., Leung, K. Y., Byers, H. L., Ward, M. A., Price, C., Bird, I. N., Perera, T., Kellie, S., Williamson, R., Anderton, B. H., and Reynolds, C. H. (2011) Tyrosine Phosphorylation of Tau by the Src Family Kinases Lck and Fyn. *Mol Neurodegener* **6**

18. Derkinderen, P., Scales, T. M. E., Hanger, D. P., Leung, K. Y., Byers, H. L., Ward, M. A., Lenz, C., Price, C., Bird, I. N., Perera, T., Kellie, S., Williamson, R., Noble, W., Van Etten, R. A., Leroy, K., Brion, J. P., Reynolds, C. H., and Anderton, B. H. (2005) Tyrosine 394 is phosphorylated in Alzheimer's paired helical filament Tau and in fetal Tau with c-Abl as the candidate tyrosine kinase. *J Neurosci* **25**, 6584-6593

19. Tremblay, M. A., Acker, C. M., and Davies, P. (2010) Tau phosphorylated at tyrosine 394 is found in Alzheimer's disease tangles and can be a product of the Abl-related kinase, Arg. *J Alzheimers Dis* **19**, 721-733

20. Lebouvier, T., Scales, T. M. E., Hanger, D. P., Geahlen, R. L., Lardeux, B., Reynolds, C. H., Anderton, B. H., and Derkinderen, P. (2008) The microtubule-associated protein Tau is phosphorylated by Syk. *Bba-Mol Cell Res* **1783**, 188-192

21. Li, C., and Götz, J. (2018) Pyk2 is a novel Tau tyrosine kinase that is regulated by the tyrosine kinase fyn. *Journal of Alzheimer's Disease* **64**, 205-221

22. Sato, S., Cerny, R. L., Buescher, J. L., and Ikezu, T. (2006) Tau-tubulin kinase 1 (TTBK1), a neuron-specific Tau kinase candidate, is involved in Tau phosphorylation and aggregation. *J Neurochem* **98**, 1573-1584

23. Lebouvier, T., Scales, T. M., Williamson, R., Noble, W., Duyckaerts, C., Hanger, D. P., Reynolds, C. H., Anderton, B. H., and Derkinderen, P. (2009) The microtubule-associated protein Tau is also phosphorylated on tyrosine. *Journal of Alzheimer's Disease* **18**, 1-9

24. Alvarez, A. R., Sandoval, P. C., Leal, N. R., Castro, P. U., and Kosik, K. S. (2004) Activation of the neuronal c-Abl tyrosine kinase by amyloid-β-peptide and reactive oxygen species. *Neurobiology of Disease* **17**, 326-336

25. Khatri, A., Wang, J., and Pendergast, A. M. (2016) Multifunctional Abl kinases in health and disease. *J Cell Sci* **129**, 9-16

26. Schlatterer, S. D., Acker, C. M., and Davies, P. (2011) c-Abl in Neurodegenerative Disease. *J Mol Neurosci* **45**, 445-452

27. von Bergen, M., Friedhoff, P., Biernat, J., Heberle, J., Mandelkow, E. M., and Mandelkow, E. (2000) Assembly of Tau protein into Alzheimer paired helical filaments depends on a local sequence motif (306VQIVYK311) forming β structure. *Proceedings of the National Academy of Sciences* **97**, 5129-5134

28. Perez, M., Arrasate, M., Montejo De Garcini, E., Munoz, V., and Avila, J. (2001) In vitro assembly of Tau protein: mapping the regions involved in filament formation. *Biochemistry-Us* **40**, 5983-5991

29. Naruto, K., Minoura, K., Okuda, R., Taniguchi, T., In, Y., Ishida, T., and Tomoo, K. (2010) Interplay between I308 and Y310 residues in the third repeat of microtubule-binding domain is essential for Tau filament formation. *FEBS Letters* **584**, 4233-4236

30. Sogawa, K., Okuda, R., In, Y., Ishida, T., Taniguchi, T., Minoura, K., and Tomoo, K. (2012) C–H… π interplay between Ile308 and Tyr310 residues in the third repeat of microtubule binding domain is indispensable for self-assembly of three-and four-repeat Tau. *The Journal of Biochemistry* **152**, 221-229

31. Scaramozzino, F., Peterson, D. W., Farmer, P., Gerig, J. T., Graves, D. J., and Lew, J. (2006) TMAO Promotes Fibrillization and Microtubule Assembly Activity in the C-Terminal Repeat Region of Tau. *Biochemistry-Us* **45**, 3684-3691

32. Inoue, M., Kaida, S., Nakano, S., Annoni, C., Nakata, E., Konno, T., and Morii, T. (2014) Phosphorylation regulates fibrillation of an aggregation core peptide in the second repeat of microtubule-binding domain of human Tau. *Bioorganic & Medicinal Chemistry* **22**, 6471-6480

33. Nishiura, C., Takeuchi, K., Minoura, K., Sumida, M., Taniguchi, T., Tomoo, K., and Ishida, T. (2009) Importance of Tyr310 residue in the third repeat of microtubule binding domain for filament formation of Tau protein. *The Journal of Biochemistry* **147**, 405-414

34. Hirata, A., Sugimoto, K., Konno, T., and Morii, T. (2007) Amyloid-forming propensity of the hydrophobic non-natural amino acid on the fibril-forming core peptide of human Tau. *Bioorganic & Medicinal Chemistry Letters* **17**, 2971-2974

35. Sogawa, K., Minoura, K., In, Y., Ishida, T., Taniguchi, T., and Tomoo, K. (2014) CH–π interaction in VQIVYK sequence elucidated by NMR spectroscopy is essential for PHF formation of Tau. *Peptide Science* **102**, 288-295

36. Von Bergen, M., Biernat, J., Mandelkow, E. M., and Mandelkow, E. (2001) A Hexapeptide Motif (306VQIVYK311)-forming β Structure Induces the Aggregation of Tau Protein to Paired Helical Filaments. *Alzheimer's Disease: Advances in Etiology, Pathogenesis and Therapeutics*, 631-640

37. von Bergen, M., Li, L., and Mandelkow, E. (2005) Intrinsic fluorescent detection of Tau conformation and aggregation. in *Amyloid Proteins*, Springer. pp 175-184

38. Goux, W. J., Kopplin, L., Nguyen, A. D., Leak, K., Rutkofsky, M., Shanmuganandam, V. D., Sharma, D., Inouye, H., and Kirschner, D. A. (2004) The formation of straight and twisted filaments from short Tau peptides. *Journal of Biological Chemistry* **279**, 26868-26875

39. Santa-María, I., Pérez, M., Hernández, F., Muñoz, V., Moreno, F. J., and Avila, J. (2006) In vitro Tau fibrillization: Mapping protein regions. *Biochimica et Biophysica Acta (BBA) - Molecular Basis of Disease* **1762**, 683-692

40. Inoue, M., Hirata, A., Tainaka, K., Morii, T., and Konno, T. (2008) Charge-Pairing Mechanism of Phosphorylation Effect upon Amyloid Fibrillation of Human Tau Core Peptide. *Biochemistry-Us* **47**, 11847-11857

41. Inoue, M., Tainaka, K., Hirata, A., Konno, T., and Morii, T. (2009) The amyloid fibrillization of phosphorylated human Tau core peptides. *Transactions of the Materials Research Society of Japan* **34**, 517-520

42. Lippens, G., and Gigant, B. (2019) Elucidating Tau function and dysfunction in the era of cryo-EM. *Journal of Biological Chemistry* **294**, 9316-9325

43. Shirazi, S. K., and Wood, J. G. (1993) The protein tyrosine kinase, fyn, in Alzheimer's disease pathology. *Neuroreport* **4**, 435-437

44. Yu, X., Luo, Y., Dinkel, P., Zheng, J., Wei, G., Margittai, M., Nussinov, R., and Ma, B. (2012) Cross-seeding and conformational selection between three- and four-repeat human Tau proteins. *J Biol Chem* **287**, 14950-14959

45. Wishart, D. S., Sykes, B. D., and Richards, F. M. (1991) Relationship between nuclear magnetic resonance chemical shift and protein secondary structure. *Journal of molecular biology* **222**, 311-333

46. Eliezer, D., Barré, P., Kobaslija, M., Chan, D., Li, X., and Heend, L. (2005) Residual structure in the repeat domain of Tau: echoes of microtubule binding and paired helical filament formation. *Biochemistry-Us* **44**, 1026-1036

47. Von Bergen, M., Friedhoff, P., Biernat, J., Heberle, J., Mandelkow, E.-M., and Mandelkow, E. (2000) Assembly of τ protein into Alzheimer paired helical filaments depends on a local sequence motif (306VQIVYK311) forming β structure. *Proceedings of the National Academy of Sciences* **97**, 5129-5134

48. Ait-Bouziad, N., Lv, G., Mahul-Mellier, A.-L., Xiao, S., Zorludemir, G., Eliezer, D., Walz, T., and Lashuel, H. A. (2017) Discovery and characterization of stable and toxic Tau/phospholipid oligomeric complexes. *Nature Communications* **8**, 1678

49. Elbaum-Garfinkle, S., Ramlall, T., and Rhoades, E. (2010) The role of the lipid bilayer in Tau aggregation. *Biophys J* **98**, 2722-2730

50. Jones, E. M., Dubey, M., Camp, P. J., Vernon, B. C., Biernat, J., Mandelkow, E., Majewski, J., and Chi, E. Y. (2012) Interaction of Tau protein with model lipid membranes induces Tau structural compaction and membrane disruption. *Biochemistry-Us* **51**, 2539-2550

51. Barré, P., and Eliezer, D. (2006) Folding of the repeat domain of Tau upon binding to lipid surfaces. *Journal of molecular biology* **362**, 312-326

52. Georgieva, E. R., Xiao, S., Borbat, P. P., Freed, J. H., and Eliezer, D. (2014) Tau binds to lipid membrane surfaces via short amphipathic helices located in its microtubule-binding repeats. *Biophys J* **107**, 1441-1452

53. Barré, P., and Eliezer, D. (2013) Structural transitions in Tau k18 on micelle binding suggest a hierarchy in the efficacy of individual microtubule-binding repeats in filament nucleation. *Protein Sci* **22**, 1037-1048

54. Sayas, C. L., Medina, M., Cuadros, R., Ollá, I., García, E., Pérez, M., Ferrer, I., Hernández, F., and Avila, J. (2019) Role of Tau N-terminal motif in the secretion of human Tau by End Binding proteins. *Plos One* **14**, e0210864

55. Derisbourg, M., Leghay, C., Chiappetta, G., Fernandez-Gomez, F.-J., Laurent, C., Demeyer, D., Carrier, S., Buée-Scherrer, V., Blum, D., Vinh, J., Sergeant, N., Verdier, Y., Buée, L., and Hamdane, M. (2015) Role of the Tau N-terminal region in microtubule stabilization revealed by new endogenous truncated forms. *Scientific Reports* **5**, 9659

56. Barbier, P., Zejneli, O., Martinho, M., Lasorsa, A., Belle, V., Smet-Nocca, C., Tsvetkov, P. O., Devred, F., and Landrieu, I. (2019) Role of Tau as a Microtubule-Associated Protein: Structural and Functional Aspects. *Frontiers in Aging Neuroscience* **11**

57. Fitzpatrick, A. W. P., Falcon, B., He, S., Murzin, A. G., Murshudov, G., Garringer, H. J., Crowther, R. A., Ghetti, B., Goedert, M., and Scheres, S. H. W. (2017) Cryo-EM structures of Tau filaments from Alzheimer's disease. *Nature* **547**, 185-190

58. Falcon, B., Zhang, W., Murzin, A. G., Murshudov, G., Garringer, H. J., Vidal, R., Crowther, R. A., Ghetti, B., Scheres, S. H. W., and Goedert, M. (2018) Structures of filaments from Pick's disease reveal a novel Tau protein fold. *Nature* **561**, 137-140

59. Falcon, B., Zivanov, J., Zhang, W., Murzin, A. G., Garringer, H. J., Vidal, R., Crowther, R. A., Newell, K. L., Ghetti, B., Goedert, M., and Scheres, S. H. W. (2019) Novel Tau filament fold in chronic traumatic encephalopathy encloses hydrophobic molecules. *Nature* **568**, 420-423

60. Duka, V., Lee, J.-H., Credle, J., Wills, J., Oaks, A., Smolinsky, C., Shah, K., Mash, D. C., Masliah, E., and Sidhu, A. (2013) Identification of the Sites of Tau Hyperphosphorylation and Activation of Tau Kinases in Synucleinopathies and Alzheimer's Diseases. *PLOS ONE* **8**, e75025

61. Bhaskar, K., Hobbs, G. A., Yen, S. H., and Lee, G. (2010) Tyrosine phosphorylation of Tau accompanies disease progression in transgenic mouse models of Tauopathy. *Neuropath Appl Neuro* **36**, 462-477

62. Wood, J. G., and Zinsmeister, P. (1991) Tyrosine phosphorylation systems in Alzheimer's disease pathology. *Neuroscience Letters* **121**, 12-16

63. Shapiro, I. P., Masliah, E., and Saitoh, T. (1991) Altered Protein Tyrosine Phosphorylation in Alzheimer's Disease. *J Neurochem* **56**, 1154-1162

64. Vega, I. E., Cui, L., Propst, J. A., Hutton, M. L., Lee, G., and Yen, S. H. (2005) Increase in Tau tyrosine phosphorylation correlates with the formation of Tau aggregates. *Mol Brain Res* **138**, 135-144

65. Ho, G. J., Hashimoto, M., Adame, A., Izu, M., Alford, M. E., Thal, L. J., Hansen, L. A., and Masliah, E. (2005) Altered p59(Fyn) kinase expression accompanies disease progression in Alzheimer's disease: implications for its functional role. *Neurobiology of Aging* **26**, 625-635

66. Williamson, R., Scales, T., Clark, B. R., Gibb, G., Reynolds, C. H., Kellie, S., Bird, I. N., Varndell, I. M., Sheppard, P. W., Everall, I., and Anderton, B. H. (2002) Rapid tyrosine phosphorylation of neuronal proteins including Tau and focal adhesion kinase in response to amyloid-β peptide exposure: Involvement of src family protein kinases. *J Neurosci* **22**, 10-20

67. Morris, M., Knudsen, G. M., Maeda, S., Trinidad, J. C., Ioanoviciu, A., Burlingame, A. L., and Mucke, L. (2015) Tau post-translational modifications in wild-type and human amyloid precursor protein transgenic mice. *Nat Neurosci* **18**, 1183-+

68. Harbison, N. W., Bhattacharya, S., and Eliezer, D. (2012) Assigning Backbone NMR Resonances for Full Length Tau Isoforms: Efficient Compromise between Manual Assignments and Reduced Dimensionality. *Plos One* **7**

69. Barghorn, S., Biernat, J., and Mandelkow, E. (2005) Purification of Recombinant Tau Protein and Preparation of Alzheimer-Paired Helical Filaments In Vitro. in *Amyloid Proteins: Methods and Protocols* (Sigurdsson, E. M. ed.), Humana Press, Totowa, NJ. pp 35-51

70. Seeliger, M. A., Young, M., Henderson, M. N., Pellicena, P., King, D. S., Falick, A. M., and Kuriyan, J. (2005) High yield bacterial expression of active c-Abl and c-Src tyrosine kinases. *Protein Sci* **14**, 3135-3139

71. Ackmann, M., Wiech, H., and Mandelkow, E. (2000) Nonsaturable binding indicates clustering of Tau on the microtubule surface in a paired helical filament-like conformation. *Journal of Biological Chemistry* **275**, 30335-30343

72. Hong, M., Zhukareva, V., Vogelsberg-Ragaglia, V., Wszolek, Z., Reed, L., Miller, B. I., Geschwind, D. H., Bird, T. D., McKeel, D., and Goate, A. (1998) Mutation-specific functional impairments in distinct Tau isoforms of hereditary FTDP-17. *Science* **282**, 1914-1917

73. Gustke, N., Trinczek, B., Biernat, J., Mandelkow, E.-M., and Mandelkow, E. (1994) Domains of Tau protein and interactions with microtubules. *Biochemistry* **33**, 9511-9522

74. Ercan, E., Eid, S., Weber, C., Kowalski, A., Bichmann, M., Behrendt, A., Matthes, F., Krauss, S., Reinhardt, P., Fulle, S., and Ehrnhoefer, D. E. (2017) A validated antibody panel for the characterization of Tau post-translational modifications. *Mol Neurodegener* **12**, 87

75. Zhang, W., Tarutani, A., Newell, K. L., Murzin, A. G., Matsubara, T., Falcon, B., Vidal, R., Garringer, H. J., Shi, Y., and Ikeuchi, T. (2019) Novel Tau filament fold in corticobasal degeneration, a four-repeat Tauopathy. *BioRxiv*, 811703

76. Zhang, W., Falcon, B., Murzin, A. G., Fan, J., Crowther, R. A., Goedert, M., and Scheres, S. H. (2019) Heparin-induced Tau filaments are polymorphic and differ from those in Alzheimer's and Pick's diseases. *Elife* **8**, e43584

FOOTNOTES

The abbreviations used are:

Abl Abelson murine leukemia viral oncogene homolog 1

AD Alzheimer's disease

Arg Abelson tyrosine-protein kinase 2

BPS brain phosphatidylserine

CBD corticobasal degeneration

CD circular dichroism

CET chronic traumatic encephalopathy

EM electron microscopy

ESI/MS electrospray ionisation mass spectrometry

fPS fluorescent phospholipids

FTDP-17 frontotemporal dementia with parkinsonism linked to chromosome 17

GTP guanosine triphosphate

HSCQS heteronuclear single quantum coherence spectroscopy

LC−MS liquid chromatography–mass spectrometry

MAPF microtubule−associated protein fraction

MS/MS tandem mass spectrometry

MT microtubule

MTBD microtubule-binding domain

MTBR microtubule-binding region

NBD nitrobenzoxadiazole

NFT neurofibrillary tangle

NMR nuclear magnetic resonance

PD Parkinson's disease

pS phospho-serine

PSP progressive supranuclear palsy

pT phospho-threonines

PTM post-translational modification

pY phospho-tyrosine

RP−HPLC reversed phase high-performance liquid chromatography

S.E.M standard error of measurement

SDS-PAGE sodium dodecyl sulphate-polyacrylamide gel electrophoresis

SP spectral count

ssi secondary shift index

Syk Spleen tyrosine kinase

ThT thioflavin T

TTBK1 Tau tubulin kinase 1

UPLC ultra performance liquid chromatography

WT wild-type